

Coherent Ion Acceleration Using Beating  
Electrostatic Waves

FINAL REPORT

9/1/2004

to the US Air Force Office of Scientific Research

GRANT NUMBER: F49620-02-1-0009

Start date:08/31/02

End date:9/1/04

PI: Prof. Edgar Choueiri

Graduate Student: Rostislav Spektor

Electric Propulsion and Plasma Dynamics Lab (EPPDyL)

Applied Physics Group

MAE Dept., Princeton University

Princeton NJ 08544

Phone: (609) 258 5220 Fax: (609) 258 6875

E-mail: choueiri@princeton.edu

20050519 118

**REPORT DOCUMENTATION PAGE**

AFRL-SR-AR-TR-05-

The public reporting burden for this collection of information is estimated to average 1 hour per response, including the time for gathering and maintaining the data needed, and completing and reviewing the collection of information. Send comments regarding this burden estimate or any other aspect of this collection of information, including suggestions for reducing the burden, to Department of Defense, Washington Headquarters Service (0704-0188), 1215 Jefferson Davis Highway, Suite 1204, Arlington, VA 22202-4302. Respondents should be aware that notwithstanding any other notice that may appear hereon, it does not display a currently valid OMB control number. **PLEASE DO NOT RETURN YOUR FORM TO THE ABOVE ADDRESS.**

0165

1. REPORT DATE (DD-MM-YYYY) 01092004		2. REPORT TYPE Final Report		3. DATES COVERED (From - To) 31 Aug 2002 - 1 Sep 2004	
4. TITLE AND SUBTITLE  Coherent Ion Acceleration Using Beating Electrostatic Waves				5a. CONTRACT NUMBER	
				5b. GRANT NUMBER  F49620-02-1-0009	
				5c. PROGRAM ELEMENT NUMBER	
6. AUTHOR(S)  Professor Edgar Choueiri				5d. PROJECT NUMBER	
				5e. TASK NUMBER	
				5f. WORK UNIT NUMBER	
7. PERFORMING ORGANIZATION NAME(S) AND ADDRESS(ES) Applied Physics Group MAE Department Princeton University Princeton NJ 08544				8. PERFORMING ORGANIZATION REPORT NUMBER	
9. SPONSORING/MONITORING AGENCY NAME(S) AND ADDRESS(ES) USAF/AFRL AFOSR 801 N. Randolph Street Arlington VA 22203 NA				10. SPONSOR/MONITOR'S ACRONYM(S)  AFOSR	
				11. SPONSOR/MONITOR'S REPORT NUMBER(S)	
12. DISTRIBUTION/AVAILABILITY STATEMENT  Distribution Statement A. Approved for public release; distribution is unlimited.					
13. SUPPLEMENTARY NOTES					
14. ABSTRACT The results obtained from AFOSR-sponsored study on a new ion acceleration using beating electrostatic waves. Unlike previously known methods of energizing plasmas with electrostatic waves, and which accelerate only ions whose initial velocities are above a certain threshold (close to the waves velocity), the new mechanism can accelerate ions with arbitrarily small initial velocities. This results in significant improvements to the acceleration/heating efficiency (by as much as 45%) over previous techniques. The benefits to the state of the art of space propulsion stem from the high efficiency of the new mechanism, its thresholdless nature and its capabilities of producing high ion energies and its electrodeless character. In summary project accomplished the following: 1. Demonstrated theoretically that a new highly efficient ion acceleration mechanism by heating electrostatic (ES) waves is real and is a fundamental phenomenon that occurs only under specific conditions. 2. Studied using Monte Carlo simulations the effects of collisions (that would occur in a real low temperature plasma) on the ion acceleration mechanism and found that collisions can enhance the effects due to scattering of ions out of the forbidden region of phase space. 3. Designed and constructed a dedicated experiment to study the new ion acceleration mechanism.					
15. SUBJECT TERMS					
16. SECURITY CLASSIFICATION OF:			17. LIMITATION OF ABSTRACT	18. NUMBER OF PAGES	19a. NAME OF RESPONSIBLE PERSON
a. REPORT	b. ABSTRACT	c. THIS PAGE			19b. TELEPHONE NUMBER (Include area code)
U	U	U	UU	57	

# Contents

<b>1 Ion Acceleration by Beating Electrostatic Waves: Domain of Allowed Acceleration</b>	<b>6</b>
1.1 Introduction	6
1.2 Analytical Formulation	7
1.3 Single Wave Interaction	11
1.4 Multiple Wave Interaction	12
1.5 Topology of the Phase Diagram	16
1.6 Critical Points	17
1.7 Beating Waves (On-Resonance)	21
1.8 Summary and Concluding Remarks	22
1.9 APPENDIX: $S_6^{\nu_i, \nu_j}(\rho)$ Term Simplification	24
<b>2 Effects of Ion Collisions on Ion Acceleration</b>	<b>26</b>
2.1 Introduction	26
2.2 Single Particle Model	27
2.3 Including Collisions	30
2.3.1 Overall implementation	30
2.3.2 Momentum exchange during a collision	30
2.3.3 Moving the particles	32
2.4 Simulation	32
2.4.1 Phase diagrams	32
2.4.2 Energy Evolution	32
2.5 Conclusions	34
<b>3 Beating Waves Experiment: Excitation of Ion Cyclotron Waves and Demonstration of Ion Acceleration</b>	<b>36</b>
3.1 Introduction	36
3.2 Review of previous work	37
3.3 Experimental setup	39
3.3.1 Vacuum Chamber	39
3.3.2 Plasma Source	41
3.3.3 Beating Waves Antenna	41
3.4 Diagnostics	42
3.5 Wave launching	44

3.6	Dispersion relation measurement . . . . .	46
3.7	Conclusions regarding ES Wave Excitation . . . . .	49
3.8	Demonstration of Ion Acceleration . . . . .	49

## SYNOPSIS

In this final technical report we document, in three chapters, the results obtained from our AFOSR-sponsored study on a new ion acceleration using beating electrostatic waves.

Unlike previously known methods of energizing plasmas with electrostatic waves, and which accelerate only ions whose initial velocities are above a certain threshold (close to the waves velocity), the new mechanism can accelerate ions with arbitrarily small initial velocities (as illustrated in Fig. (1)). This results in significant improvements to the acceleration/heating efficiency (by as much as 45%) over previous techniques. The benefits to the state of the art of space propulsion stem from the high efficiency of the new mechanism, its thresholdless nature and its capabilities of producing high ion energies and its electrodeless character.

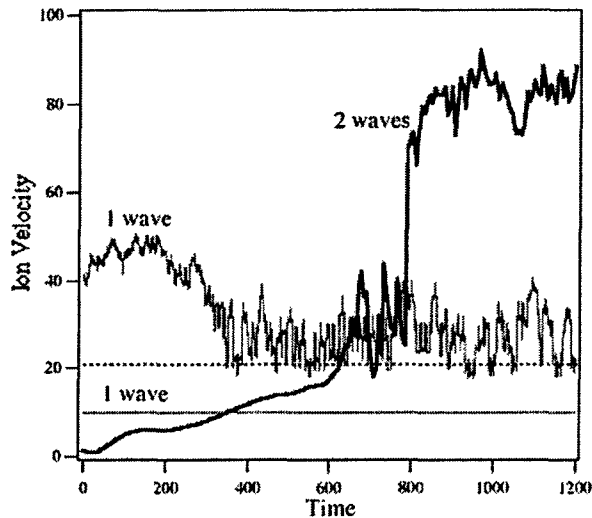


Figure 1: Calculation from first principles (using Hamiltonian formulation) of ion acceleration by two beating electrostatic waves (red curve) compared to the effect of a single wave (blue curve). Unlike the single wave case, the 2-wave interaction accelerates ions whose initial velocity is below the classical threshold (dotted horizontal line) to significantly high velocities. The thresholdless nature and efficiency of this acceleration mechanism make it most promising for propulsion applications.

In summary we have accomplished the following:

1. Demonstrated theoretically that a new highly efficient ion acceleration mechanism by beating electrostatic (ES) waves is real and is a fundamental phenomenon that occurs only under specific conditions that were not

known before. We derived, from first principles, the fundamental necessary *and* sufficient conditions for the acceleration mechanism to occur.

2. We studied using Monte Carlo simulations the effects of collisions (that would occur in a real low temperature plasma) on the ion acceleration mechanism and found that collisions can enhance the effects due to scattering of ions out of the forbidden region of phase space.
3. We designed and constructed a dedicated experiment to study the new ion acceleration mechanism. We were able to launch and beat ion cyclotron waves in an argon plasma produced by a helicon source and, using a dedicated state-of-the-art LIF diagnostic system (acquired through a recent DURIP grant), **we were able to provide the first laboratory demonstration of the existence of this new ion acceleration mechanism.**

This final technical report consists of three chapters summarized below.

In **Chapter 1** the conditions under which a magnetized ion can be accelerated through a nonlinear interaction with a pair of beating electrostatic waves are explored. The electric field of the beating waves can, under some conditions, accelerate ions from arbitrarily low initial velocity in stark contrast with the well-known nonlinear threshold criteria for ion acceleration by a single wave. A numerical investigation of the fundamental dynamics led to the identification of critical points on the Poincaré cross-section. A second-order perturbation analysis was carried out to approximate the location of these critical points and define the domains of allowed and forbidden acceleration. It is shown that for an ion to be significantly energized, the Hamiltonian must be outside the energy barrier defined by the location of the elliptic and hyperbolic critical points. Despite the restriction on the Hamiltonian, an ion with arbitrarily low initial velocity may benefit from this acceleration mechanism. The resulting domain of allowed acceleration is significantly larger than that of ion acceleration by either single or non-beating waves.

In **Chapter 2** a numerical model of the nonlinear interaction between beating electrostatic waves and magnetized ions, including collisions, is presented. Previous studies of the beating electrostatic waves (BEW) interacting with a single ion showed the ability of this mechanism to accelerate ions from arbitrarily low initial velocities, and have revealed the fundamental conditions for this interaction to occur. The present study extends the analysis to a large number of ions and includes ion-ion collisions. The numerical investigation combines a dynamical description for the ion-wave interaction and a Monte Carlo simulation of the collisions. Despite the thermalization role of collisions BEW acceleration was found to yield larger heating rate and higher particle energies than the better known interaction with the single electrostatic wave (SEW).

In **Chapter 3** we report on our experiments that demonstrate the existence of the new acceleration mechanism. We first report on the excitation and propagation of Electrostatic Ion Cyclotron (EIC) waves in an rf-sustained argon plasma and our measurements of the sought dispersion relations. Such waves

were used to study the beating waves ion acceleration mechanism as reported in the last section of the chapter. The waves are excited by an antenna consisting of two parallel metal plates inserted at the edge of a plasma column with their surface normal perpendicular to magnetic field. The plates can be driven in or out of phase. The in-phase configuration couples better to plasma. It is shown that EIC waves launched at frequencies between  $\omega_{ci}$  and  $10\omega_{ci}$  propagate with little damping at an angle between  $82^\circ$  and  $86^\circ$  with respect to the magnetic field. The amplitude of the excited waves can be optimized by properly matching the impedance of the driving circuit to the plasma and choosing the right plasma conditions. The dispersion relation was measured using a phase-delay technique and was found to be in good agreement with the theoretical EIC dispersion relation over a wide range of frequencies. We conclude that chapter and the report with **the first laboratory demonstration of the existence of the new ion acceleration mechanism** by directly measuring a significant (up to 40%) increase in the perpendicular ion energy.

**Acknowledgements** This work has been carried out under contract from the US Air Force Office of Scientific Research (AFOSR) under Grant number F49620-02-1-0009. Technical Contract Manager: Dr. Mitat Birkan. Mr. Robert Sorenson provided valuable assistance in developing the experiment. The authors are thankful to professor Scime of West Virginia University for equipment loaned and for his invaluable assistance in setting up the laser-induced fluorescence (LIF) diagnostic which we acquired through a recent AFOSR-DURIP grant.

## Chapter 1

# Ion Acceleration by Beating Electrostatic Waves: Domain of Allowed Acceleration

### 1.1 Introduction

Stochastic heating of a magnetized ion by a single propagating electrostatic (ES) wave has been extensively studied [1, 2, 3, 4]. Using first-order perturbation theory Karney [3, 5] was able to derive analytical expressions approximating overall nonlinear dynamics of an ion interacting with a single ES wave. That work revealed the existence of a threshold for the initial ion energy below which the particle cannot gain net energy from the ES wave. Skiff *et al.* validated these findings experimentally [6]. The threshold is essentially the lower bound of a nonlinearly broadened resonance condition between the ion velocity and wave phase velocity. Ions with initial velocities below this threshold will not gain net energy and their motion will remain coherent, while ions moving slightly faster than the wave will be accelerated stochastically. Thus the threshold separates two regions of phase space: a *regular* (or coherent) motion region of low energies below the threshold and a *stochastic* one - above the threshold. Nonlinear ion acceleration by a single wave is therefore always a stochastic process.

In 1998 Benisti *et al.* described a new mechanism for nonlinear ion acceleration by ES waves [7, 8]. The scheme requires *pairs* of ES waves that obey a beating criterion: their frequencies must differ by an integer number of the ion cyclotron frequency. In essence the beating of two or more ES waves creates a propagating electric field structure having a low-frequency amplitude envelope. Slow ions are first accelerated *coherently* through interaction with this envelope and are then further accelerated *stochastically* by the higher harmonics of the

beat wave. Under such conditions the single-wave theory threshold disappears and *regular* and *stochastic* regions of phase space become connected allowing ions with arbitrary small initial velocities to obtain high energies through coherent acceleration followed by stochastic energization. Consequently, this nonlinear interaction may result in a more efficient acceleration mechanism than is possible from the interaction with a single wave. This new acceleration scheme has been advanced as a possible explanation for the ionospheric ion acceleration observed during the Topaz 3 [9] rocket experiments. An acceleration mechanism that promises to energize a larger portion of the ion distribution function may be promising to many applications where the efficiency of ion heating is of prime importance, such as in spacecraft plasma propulsion.

A preliminary numerical exploration [10] of this mechanism revealed that there are many cases for which the beating criterion does not lead to ion acceleration. This hinted to the possibility that the criterion is necessary but not sufficient.

In this study we attempt, using analytical and numerical techniques, to define the necessary *and* sufficient conditions for the acceleration of the magnetized ion through nonlinear interaction with a pair of propagating electrostatic waves. In particular, we use second-order perturbation theory and numerical integration to analyze the nonlinear dynamics by finding the location of the critical points [11] of the motion on a Poincaré cross-section [12]. These critical points were not observed in previous studies [7, 8] since they were limited to the analysis of a single trajectory (i.e. single initial condition) in a given Poincaré cross-section. The location of these critical points allows us to define the initial conditions for the Hamiltonian and the ion's velocity required for a magnetized ion to be energized by a pair of beating waves.

In section 1.2 we overview the analytical formulation of the problem. In order to give context to our study we review in section 1.3 the better-known dynamics of a magnetized ion interacting with a single ES wave. This is followed in section 1.4 by an overview of the fundamental features of the new mechanism that relies on beating waves. In the remaining sections we seek expressions for the location of the critical points of the motion which amount to a definition of the domains of allowed and forbidden acceleration.

## 1.2 Analytical Formulation

We start by defining the coordinate axis as shown in Fig. 1.1. Here we have a single ion of mass  $m$  and charge  $q$  in a constant and homogeneous magnetic field,  $B\hat{z}$ . This ion interacts with a packet of electrostatic waves that propagate in the positive  $x$  direction. Since we take the waves to be purely electrostatic the wave-number  $k_i$  is parallel to the electric field  $E_i$  of each of these waves. The dynamics of the single ion in Fig. 1.1 is described by the following equation

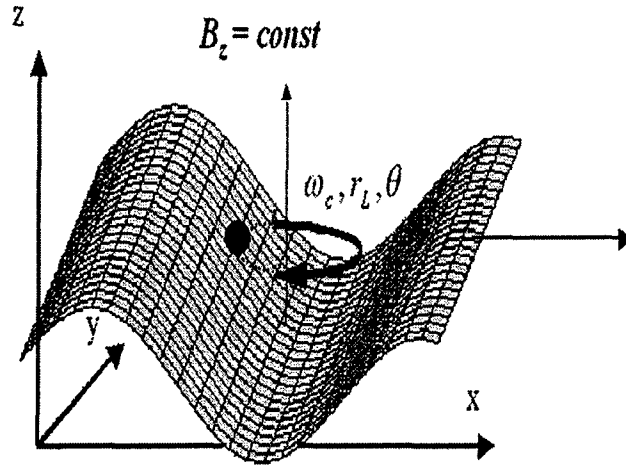


Figure 1.1: A single ion of charge  $q$  and mass  $m$  in a constant homogeneous magnetic field  $B\hat{z}$  interacts with a spectrum of electrostatic waves whose wave-number and electric field direction is parallel to the  $x$ -axis.

of motion [13, 7]:

$$\frac{d^2x}{dt^2} + \omega_c^2 x = \frac{q}{m} \sum_i E_i \sin(k_i x - \omega_i t + \varphi_i), \quad (1.1)$$

where  $\omega_c = qB/m$  is the ion cyclotron frequency and  $\varphi_i$  is the phase angle of each wave. The corresponding Hamiltonian for the system is [7]

$$\bar{H} = \rho^2/2 + \sum_i \frac{\varepsilon_i}{\kappa_i} \cos(\kappa_i \rho \sin \theta - \nu_i \tau + \varphi_i). \quad (1.2)$$

In writing Eq. (1.2) we have used the fact that the system is periodic, and transformed the Hamiltonian into normalized action-angle coordinate system [14], where  $\kappa_i = k_i/k_1$ ,  $\nu_i = \omega_i/\omega_c$ ,  $\tau = \omega_c t$ ,  $\varepsilon_i = (k_1 q E_i)/(m \omega_c^2)$ ,  $\rho^2 = X^2 + \dot{X}^2$ , and  $X = k_1 x$ ,  $\dot{X} = dX/d\tau$ , so that  $X = \rho \sin \theta$ ,  $\dot{X} = \rho \cos \theta$ . The action-angle coordinate system is a special case of polar coordinates [12]. In our context  $\theta$  corresponds to the cyclotron phase angle measured clockwise from the  $y$ -axis, as indicated on Fig. 1.1, while  $\rho$  is the normalized Larmor radius which, in a constant magnetic field, represents the normalized velocity (perpendicular to the magnetic field) of the magnetized particle undergoing cyclotron motion in the  $xy$  plane.

Benisti *et al.* [7] defined a criterion for particle acceleration by multiple ES waves. They showed that for regular and stochastic regions to be connected it is necessary (but, as we shall see, not sufficient) to have at least one pair of ES

waves such that

$$\omega_2 - \omega_1 = n\omega_c, \quad (1.3)$$

where  $n$  is an integer. They also report that acceleration is more vigorous for  $n \leq 2$ , therefore for the sake of simplicity, we limit our analysis to the case of a single pair of beating waves, such that  $n = 1$ . In addition, Ref.[7] reports that the maximum acceleration is achieved when all waves are of the same amplitude,  $\varepsilon_i = \varepsilon_j = \varepsilon$ . We also set  $\kappa_i = \kappa_j = \kappa_1$  to simplify our analysis, and since the phase angles,  $\varphi_i$ , do not play a fundamental role in this acceleration process [7] we set all  $\varphi_i = 0$ . With these simplifications the Hamiltonian (1.2) becomes

$$\bar{H} = \rho^2/2 + \varepsilon[\cos(\rho \sin \theta - \nu_i \tau) + \cos(\rho \sin \theta - \nu_j \tau)]. \quad (1.4)$$

This Hamiltonian represents two coupled oscillators: one is the gyrating ion and the other corresponds to the beating ES waves. We, therefore, can interpret  $\varepsilon$  as a coupling parameter between the two oscillators.

Two approaches are taken in this study for analyzing the system above. First, we derive the analytical solution to equation (1.4) by applying a second-order perturbation technique in conjunction with Deprit modified [15, 16] Lie transformations [12, 13], and then compare it with the results of numerical integration of equation (1.4). To obtain the numerical solution we use the fourth-order symplectic integration algorithm (SIA4) derived by Candy and Rozmus [17] who showed its superiority over fourth order Runge-Kutta algorithm for Hamiltonian periodic problems, such as ours.

A convenient way of representing both numerical and analytical solutions is to plot the resulting trajectories on a Poincaré cross-section [12]. To construct a Poincaré cross-section from the numerical integration of Eq. (1.4) we plot the point intersections of the ion trajectory in three dimensions  $(\rho, \theta, \tau)$  with the  $\rho$ - $\theta$  plane at specific time intervals. For integer values of  $\nu$  this reduces to plotting  $\rho$  vs.  $\theta$  at  $\tau = 2\pi j$ , where  $j = 0, 1, 2, \dots$  is a non-negative integer. For non-integer values of  $\nu$  precaution must be taken for proper accounting of intersection points. Since the magnetic field is constant, the normalized cyclotron radius  $\rho$  is a direct measure of the perpendicular ion velocity. Therefore Poincaré cross-sections give direct visual insight into the acceleration process.

The visual interpretation of Poincaré cross-sections is straightforward. Random point distribution corresponds to stochastic motion while regular patterns, such as lines and ellipses, will tell us that the ion dynamics is analytical (or regular). For example, if the wave amplitude,  $\varepsilon$ , is zero, Eqs. (1.1) and (1.4) reduce to a simple harmonic oscillator and for irrational values of  $\nu$  its Poincaré cross-section shows a set of horizontal lines, indicating constant velocity (which corresponds to a free ion gyrating in a constant magnetic field). Each of these lines represents an invariant of motion for a given set of initial conditions [12]. When the coupling parameter  $\varepsilon$  is not zero, we can treat the ion motion as a perturbation of these invariants.

The detailed derivation of the analytical solution for a particle interacting with a single wave can be found in Ref.[5]. However, a more generalized solution for multiple waves is obtained [12, 13, 18] through Deprit's modified Lie transformation in Refs.[7, 8]. The resulting autonomous Hamiltonian derived from Eq. (1.4) for a *non-integer* value of  $\nu$  to the second order in the perturbation,  $\varepsilon$ , is

$$\begin{aligned} H = & \varepsilon\{J_{\nu_i}(\rho) \cos(\nu_i\theta) + J_{\nu_j}(\rho) \cos(\nu_j\theta)\} \\ & + \varepsilon^2\{S_1^{\nu_i}(\rho) + S_1^{\nu_j}(\rho) \\ & + S_6^{\nu_i, \nu_j}(\rho) \cos[(\nu_j - \nu_i)\theta]\}, \end{aligned} \quad (1.5)$$

where,

$$\begin{aligned} S_1^{\nu_i}(\rho) &= \frac{1}{2\rho} \sum_{m=-\infty}^{\infty} \frac{mJ_m(\rho)J'_m(\rho)}{\nu_i - m}, \\ S_6^{\nu_i, \nu_j}(\rho) &= \frac{1}{2\rho} \left( \sum_{m=-\infty}^{\infty} \frac{mJ_m(\rho)J'_{\nu_j - \nu_i + m}(\rho)}{\nu_i - m} + \right. \\ & \left. + \sum_{m=-\infty}^{\infty} \frac{mJ_m(\rho)J'_{\nu_i - \nu_j + m}(\rho)}{\nu_j - m} \right), \end{aligned} \quad (1.6)$$

$J_m$  is the Bessel function of the first kind of order  $m$ , and  $J'$  represents the derivative of the Bessel function with respect to its argument. When  $\nu_i$  is an integer, the summations are performed over all  $m \neq \nu_i$  to avoid singularities. When  $\nu \neq$  integer, the first order terms in Eq. (1.5) disappear [7], and the equation becomes more tractable.

The Hamiltonian in Eq. (1.5) is autonomous and therefore itself is an invariant of motion. Curves of constant  $H$  in a Poincaré cross-section represent the complete analytical solution of the problem to second order. We now wish to compare the Poincaré cross-sections of the analytical solution to those obtained through numerical integration of Eq. (1.4). It should be noted that we should not expect to see any stochastic behavior on the Poincaré cross-sections obtained from the analytical solution.

As with most phase diagrams, critical points define the dynamics of motion. Since the system is not dissipative we expect to find two types of critical points: elliptic and hyperbolic. As we shall show later, the location of the critical points is the key to determining which initial conditions lead to acceleration or trapping. The task before us is to find these critical points.

We now explore particle dynamics as a function of wave amplitude and frequency, and in terms of the location of critical points on the Poincaré cross-section. Using numerical solutions we will demonstrate that when critical points are absent in the regular region of the Poincaré cross-section (as in the single wave-particle interaction), the particle will not gain net energy.

### 1.3 Single Wave Interaction

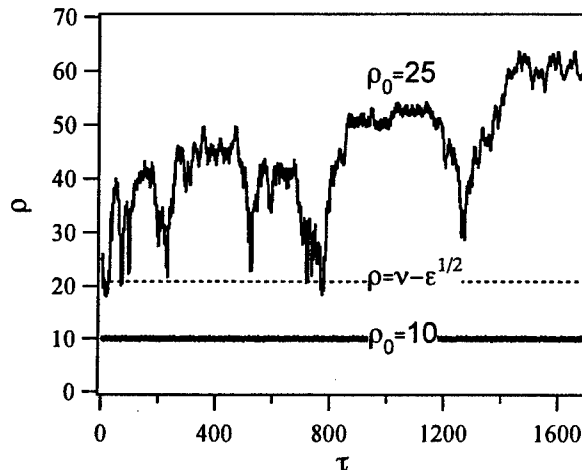


Figure 1.2: Time evolution of the normalized velocity  $\rho$  for a particle interacting with a single off-resonance wave ( $\epsilon = 10$ ,  $\nu = 24.3$ ). The threshold derived in Ref.[5] and given by Eq. (1.7) represents the boundary between the regular and stochastic domains and is shown as a horizontal dashed line. This picture is qualitatively similar to the case of the *non-beating* waves.

In this section, in order to create a context for our study, we summarize the results obtained by Karney [5, 3] for the interaction of a magnetized particle with a single electrostatic wave. When the wave frequency is exactly an integer number of the ion cyclotron frequency it is said to be an *on-resonance* wave, otherwise it is an *off-resonance* wave. In both cases Karney found that a threshold given by

$$\rho = \nu - \sqrt{\epsilon}, \quad (1.7)$$

separates the regions of regular and stochastic motion [5, 19], as shown Fig. 1.2, which illustrates for the numerical solution of the equation of the motion (1.1) a typical case ( $\epsilon = 10$ ,  $\nu = 24.3$ ). Below the threshold, indicated by the horizontal dashed line ( $\rho \sim 20$ ), we observe that the ion motion is regular and we can predict its behavior well by means of perturbation theory. More importantly, as long as the ion's initial velocity is in that region it is clear that the ion will not gain net energy from the wave [5]. When the initial velocity is above the threshold, the ion moves stochastically and eventually gains net energy, as shown by the upper trajectory in Fig. 1.2. Therefore, in the case of interaction with a single wave the ion gains energy only chaotically when its initial velocity  $\rho_0$  exceeds the threshold.

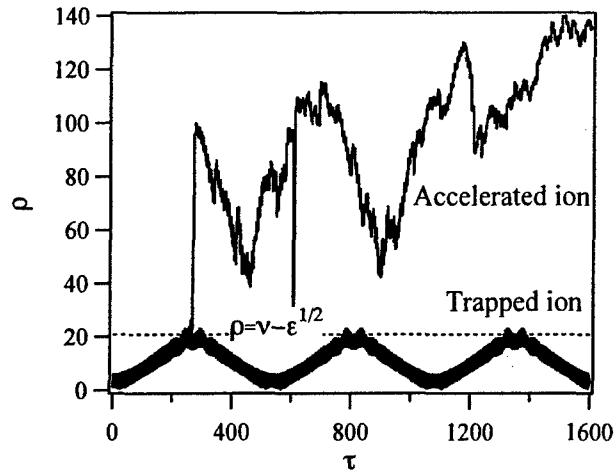


Figure 1.3: Time evolution of the normalized velocity  $\rho$  for a particle interacting with two beating waves ( $\epsilon = 10$ ,  $\nu_i = 24.3$ ,  $\nu_j = 25.3$ ). Two particle trajectories are shown, one with an ion trapped below  $\rho < \nu - \sqrt{\epsilon}$  threshold and another resulting in an accelerating ion. For both trajectories  $\rho_0$  are the same but  $\theta_0$  are different.

This is an important point and we will contrast it later with the case of beating waves where, as we shall see, the two regions of phase space can become connected under some conditions, and a particle with an arbitrarily small initial velocity in the regular region can be accelerated through the threshold to high values of  $\rho$ .

#### 1.4 Multiple Wave Interaction

One of the early investigations of two ES waves interacting with ions was done by Chia *et al.* [13, 20] who conducted an analytical study of the interaction to first order in the perturbation and found that for the waves with even-even or odd-odd combinations of frequencies  $\nu$ , there existed a vertical separatrix allowing “infinite” heating. In 1998 Benisti *et al.* [7, 8, 9] showed that to observe particle acceleration *through* the threshold boundary one needs to use perturbation theory to at least *second* order. According to their analysis, the normalized condition for the new acceleration mechanism already given by Eq. (1.3) is

$$\nu_i - \nu_j = n, \quad (1.8)$$

where  $n$  is an integer. This amounts to a wave beating condition. By analyzing a *single* ion trajectory obtained from numerical solutions of Eq. (1.1) Benisti *et*

*al.* showed that as long as condition (1.8) is satisfied the ion will gain significant energy from the waves.

Subsequently, we performed numerical investigation [10] based on the same single trajectory method and found that some ion trajectories did not lead to ion acceleration even if condition (1.8) was satisfied, as shown in Fig. 1.3. We concluded that to find the necessary and *sufficient* conditions for ion acceleration we need to examine the complete Poincaré cross-section and find the critical points of motion, as will be done in sections 1.5 and 1.6.

We first investigated the case of two electrostatic waves when condition (1.8) does not hold. The picture is qualitatively very similar to that of the single wave-particle interaction shown in Fig. 1.2. Ions with energies below some threshold maintain coherent motion and do not gain net energy. This picture can change drastically if condition (1.8) is satisfied.

As we already mentioned above, the case of the off-resonance beating waves (both  $\nu_1$  and  $\nu_2$  are not integers) provides us with much more tractable analytical expressions. Consequently, we will focus our attention on such cases. Some qualitative analysis of the on-resonance beating waves is still possible and will be done in section 1.7.

In Fig. 1.4 we show typical Poincaré cross-sections obtained by numerical integration for  $\nu_1 = 24.3$  and  $\nu_2 = 25.3$ . The panels in this figure illustrate the effect of increasing wave amplitude. The phase diagram consists of two regions, stochastic and regular, just as for the single wave interaction. However, unlike the single wave-ion interaction, the two regions are “connected”. By “connected” we mean that an ion with low initial velocity can undergo first regular and then stochastic acceleration, reaching high energies.

For low perturbation strength (low values of  $\epsilon$ ) the regular region extends to values of  $\rho$  approximately predicted by Eq. (1.7). However, as  $\epsilon$  is increased the regular region quickly shrinks to the vicinity of the elliptic critical point (designated **E** on Fig. 1.4.) Notice that the elliptic point is located at  $\rho_E \sim \nu/2$  and  $\theta_E = \pi$ . In dimensional quantities the position translates into relation between the ion velocity and the wave phase velocity,  $v_{ion} \sim -0.5\omega/k$ . Eventually, as the wave amplitude is raised above values shown on Fig. 1.4, chaotic motion dominates the phase diagram.

We now gauge how well the second-order perturbation analysis compares to the numerical solutions. Fig. 1.5 indicates a good degree of agreement between the two. Even though the detailed structure of the regular motion lines is not captured with the analytical solution, the latter does predict the position of the lower elliptic (**E**) as well as the hyperbolic point (**H**) rather well. On the other hand, our analytical approach breaks down in the stochastic region, as should be expected. Therefore the critical points shown by the analytical solution to be at  $\rho > 25$  in Fig. 1.5 (which can be said to describe a “homoclinic tangle” or “stochastic layer”) are in reality covered by the stochastic motion, as shown by the numerical solution.

However, as described in Ref.[8], even in that region of phase space the overall ion motion could be approximated by first-order orbits, for small  $\epsilon$ .

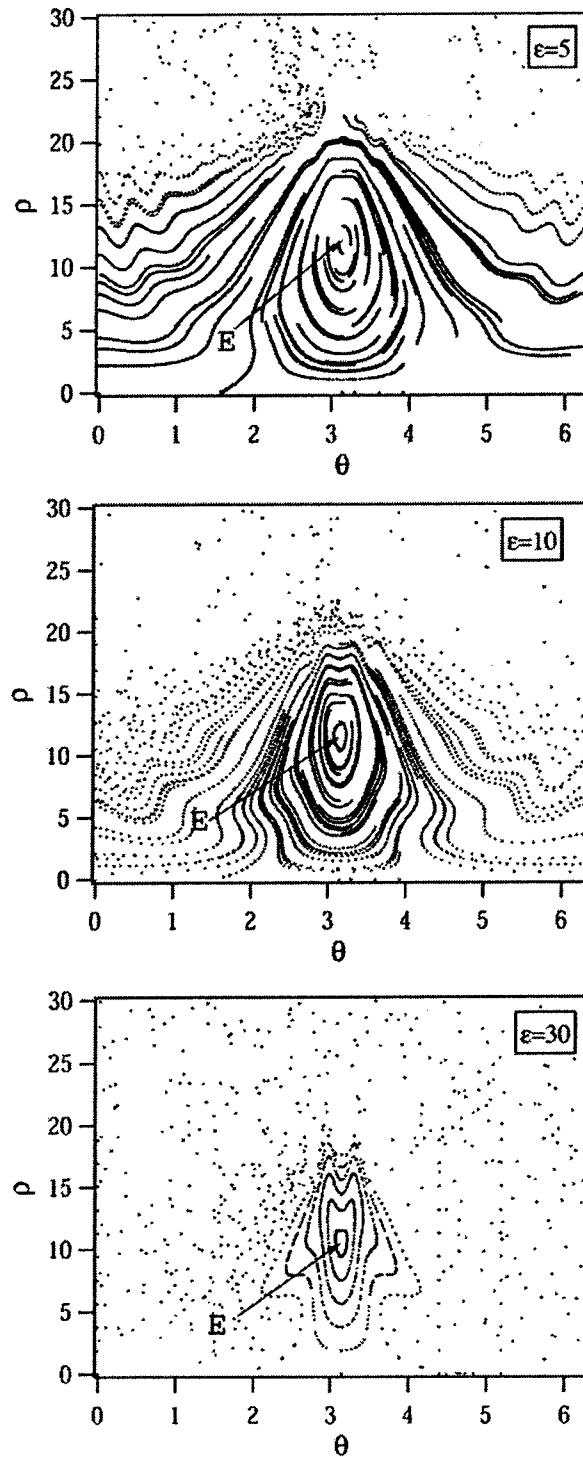


Figure 1.4: Poincaré cross-sections showing numerical solutions for a particle interacting with two beating off-resonance waves ( $\nu_i = 24.3$ ,  $\nu_j = 25.3$ ). The stochastic region occupies a greater fraction of the phase space as the wave amplitude is increased.

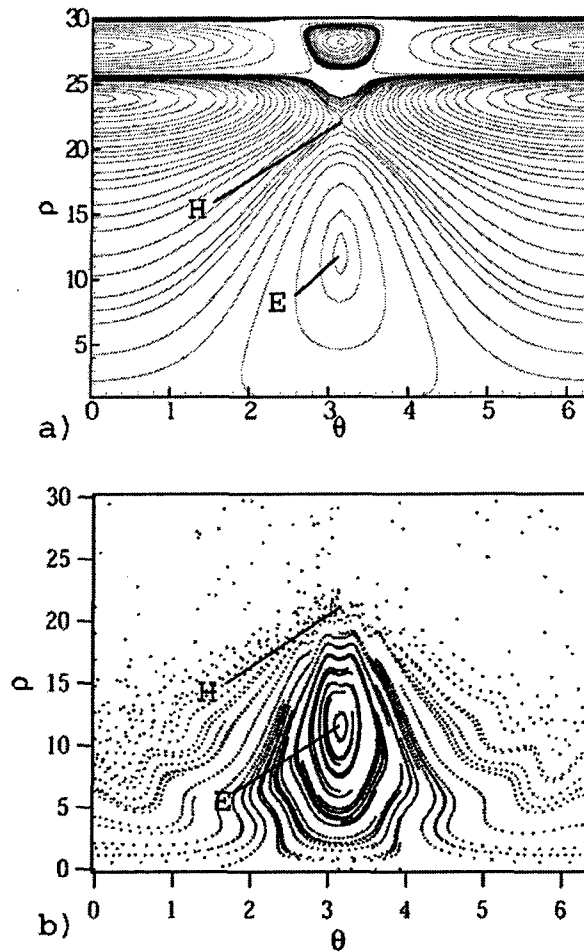


Figure 1.5: Poincaré cross-section for a particle interacting with two beating off-resonance waves ( $\epsilon = 10$ ,  $\nu_i = 24.3$ ,  $\nu_j = 25.3$ ). a) Analytical solution showing the existence of hyperbolic and elliptic points marked by **H** and **E** respectively. b) Numerical solution also showing the locations of the critical points.

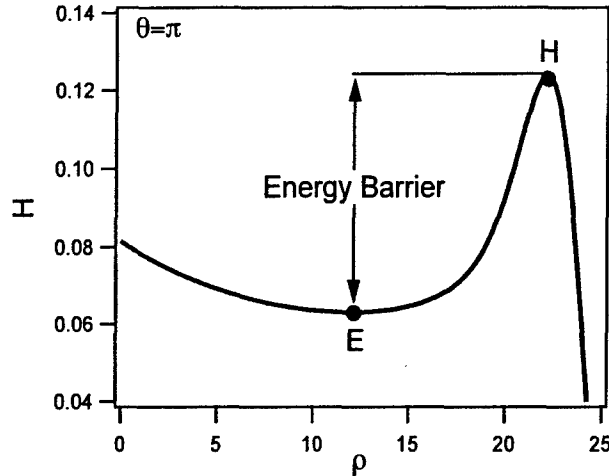


Figure 1.6: Analytical Hamiltonian as a function of  $\rho$  at  $\theta = \pi$ . The elliptic and the hyperbolic points corresponding to the ones shown in Fig. 1.5 are the minimum and the maximum of  $H$ . ( $\nu_i = 24.3$ ,  $\nu_j = 25.3$ ).

## 1.5 Topology of the Phase Diagram

As with any phase diagram, each curve on the Poincaré cross-section corresponds to a given set of initial conditions. In the case of a particle interacting with beating waves we are mainly concerned with the hyperbolic and elliptic critical points designated **H** and **E** respectively on Fig. 1.5. It is clear by tracing trajectories in Figs. 1.4 and 1.5 that an ion with Hamiltonian lying between the Hamiltonian values corresponding to points **E** and **H** does not gain net energy from the waves i.e. does not reach the stochastic region where it can be vigorously accelerated. Instead the corresponding phase space trajectories circulate around the elliptic critical point **E** or cover the full range of cyclotron phase angles ( $0 \leq \theta \leq \pi$ ) while remaining below **H**.

Other features of the Poincaré cross-section in Fig. 1.5 worth mentioning (but not central to our discussion on acceleration) are the two degenerate saddle points that can be seen at the intersection of the fourth curve (outward) from the elliptic point with the  $\theta$ -axis and the “primary” (upper) separatrix that is approximately near the eleventh curve (outward) from the elliptic point.

It is relevant to note in this context that the Hamiltonian of various trajectories increases monotonically from the Hamiltonian value at point **E** to its value at point **H**, as shown in Fig. 1.6. The figure shows the Hamiltonian as a function of  $\rho$  for  $\theta = \pi$  and illustrates that the location of the *elliptic* and the *hyperbolic* points could be found by determining the local minimum and the maximum of  $H$ .

Therefore, for given values of  $\nu_i$  and  $\varepsilon$ , the inequality

$$H_E < H(\rho_0, \theta_0) < H_H, \quad \text{with } \rho_0 < \nu - \sqrt{\varepsilon} \quad (1.9)$$

defines the *forbidden acceleration domain*, where  $H_E$  and  $H_H$  are the Hamiltonian values for the elliptic (**E**) and the hyperbolic (**H**) points, and subscript 0 refers to initial conditions. By “forbidden acceleration domain” we mean here the domain of initial conditions for which an ion cannot reach the stochastic region of phase space where it can be vigorously energized. All other ion trajectories then lie in the *allowed acceleration domain* of phase space. The ions in the allowed acceleration domain will be affected by the waves strongly. The restriction on  $\rho_0$  in Eq. (1.9) is needed because ions with  $\rho_0 \geq \nu - \sqrt{\varepsilon}$  will not be trapped in the energy barrier between the elliptic and the hyperbolic points (i.e. in the forbidden acceleration domain), as shown in Fig. 1.6.

The “trapping” criterion in Eq. (1.9) given in terms of the Hamiltonian should be contrasted with the threshold criterion for interaction with a single wave given by Eq. (1.7). It is clear that unlike the single-wave case, an ion with initial velocity  $\rho_0$  below the “threshold” can still be accelerated to high energies if the corresponding Hamiltonian is outside the range described by Eq. (1.9)

From the point of view of plasma acceleration one would like to limit the number of particles trapped in the forbidden acceleration domain ( $H_E < H(\rho_0, \theta_0) < H_H$ ). The rest of the ions gain much higher energies through first regular (if their initial energy is low) and then stochastic acceleration, as shown in Figs. 1.4 and 1.5. However, even the trapped particles can escape into the stochastic domain if we consider a collisional plasma, given that a trapped particle may gain enough energy during a collision to overcome the energy barrier, Fig. 1.6, as we have shown through particle simulations reported in Ref.[21].

## 1.6 Critical Points

To define the domains of allowed and forbidden acceleration described by Eq. (1.9) we need to find the location of the critical points **E** and **H**. We now seek analytical expressions for both.

Since both points are the extrema of the Hamiltonian, that task can be achieved by setting the time derivative of  $\rho$  and  $\theta$  to zero simultaneously [12, 11]. Utilizing Hamilton’s equations of motion in conjunction with Eqs. (1.5) and (1.6) we get

$$\dot{\rho} = \frac{\partial H}{\partial \theta} = \varepsilon \{ \nu_i J_{\nu_i}(\rho) \sin(\nu_i \theta) \quad (1.10)$$

$$+ \nu_j J_{\nu_j}(\rho) \sin(\nu_j \theta) \} \\ + \varepsilon^2 (\nu_i - \nu_j) S_6^{\nu_i, \nu_j}(\rho) \sin[(\nu_j - \nu_i)\theta] = 0,$$

$$\dot{\theta} = -\frac{\partial H}{\partial \rho} = \varepsilon \{ J'_{\nu_i}(\rho) \cos(\nu_i \theta) \quad (1.11)$$

$$+ J'_{\nu_j}(\rho) \cos(\nu_j \theta) \}$$

$$\begin{aligned}
& + \varepsilon^2 \{ S_1^{\nu_i}(\rho) + S_1^{\nu_j}(\rho) \\
& + S_6^{\nu_i, \nu_j}(\rho) \cos[(\nu_i - \nu_j)\theta] \} = 0.
\end{aligned}$$

When both wave frequencies are off-resonance ( $\nu_i, \nu_j \neq \text{integer}$ ), the equations above simplify because the first-order terms drop out, and we are able to obtain the position of critical points analytically.

For  $\nu \neq \text{integer}$ , the  $S_1^{\nu_i}(\rho)$  term in Eq. (1.6) could be simplified to an algebraic equation containing only few Bessel functions [13]:

$$\begin{aligned}
S_1^{\nu_i}(\rho) &= \frac{\pi}{8 \sin \nu_i \pi} [J_{\nu_i+1}(\rho) J_{-(\nu_i+1)}(\rho) \\
&- J_{\nu_i-1}(\rho) J_{-(\nu_i-1)}(\rho)]. \tag{1.12}
\end{aligned}$$

As a result of this simplification we can reduce the  $S_6^{\nu_i, \nu_j}(\rho)$  term down to

$$S_6^{\nu_i, \nu_j}(\rho) = \frac{\rho}{\nu_i} S_1^{\nu_i}(\rho) + \frac{\rho}{\nu_j} S_1^{\nu_j}(\rho). \tag{1.13}$$

The details of this derivation are given in the appendix. We can therefore express the Hamiltonian (1.5) in terms of the simplified  $S_1^{\nu_i}(\rho)$  function only,

$$\begin{aligned}
H &= \varepsilon^2 \left\{ \left( 1 + \frac{\rho}{\nu_i} \cos[\nu_i - \nu_j]\theta \right) S_1^{\nu_i}(\rho) \right. \\
&+ \left. \left( 1 + \frac{\rho}{\nu_j} \cos[\nu_i - \nu_j]\theta \right) S_1^{\nu_j}(\rho) \right\}. \tag{1.14}
\end{aligned}$$

As we will show later in this section our analysis breaks down for small values of  $\nu$ . Consequently we take  $\nu_i \gg 1$ , and remembering that  $n = 1$  with  $\rho/\nu_j = \rho/(\nu_i + 1) \sim \rho/\nu_i (1 - 1/\nu_i^2 + \dots)$  we can approximate  $\rho/\nu_i \sim \rho/\nu_j$ . Dropping the subscripts in  $S_1^{\nu_i}(\rho)$  we have

$$\begin{aligned}
H &= \varepsilon^2 \left[ 1 + \frac{\rho}{\nu_i} \cos(\nu_i - \nu_j)\theta \right] \times \\
&\quad \left[ S^{\nu_i}(\rho) + S^{\nu_j}(\rho) \right]. \tag{1.15}
\end{aligned}$$

Finally, we substitute Eq. (1.12) for each of the  $S_1^{\nu_i}(\rho)$  functions. Expressing everything in terms of  $\nu_i$  we get

$$\begin{aligned}
H &= \frac{\varepsilon^2 \pi}{8 \sin \nu \pi} \left( 1 + \frac{\rho}{\nu} \cos \theta \right) \\
&\quad \left[ - J_{\nu-1}(\rho) J_{-(\nu-1)}(\rho) + J_{\nu}(\rho) J_{-\nu}(\rho) \right. \\
&\quad \left. + J_{\nu+1}(\rho) J_{-(\nu+1)}(\rho) - J_{\nu+2}(\rho) J_{-(\nu+2)}(\rho) \right], \tag{1.16}
\end{aligned}$$

where we have replaced  $\nu_i$  with  $\nu$ .

We are now ready to find the position of points **E** and **H**. From Eq. (1.10) as well as from Figs. 1.4 and 1.5 we see that these points lie at  $\theta = \pi$ . This reduces equations (1.10) and (1.11) to

$$\begin{aligned} \frac{\partial}{\partial \rho} \left(1 - \frac{\rho}{\nu}\right) L(\rho) &= 0, \quad \text{where} & (1.17) \\ L(\rho, \nu) &= -J_{\nu-1}(\rho)J_{-(\nu-1)}(\rho) + J_{\nu}(\rho)J_{-\nu}(\rho) \\ &+ J_{\nu+1}(\rho)J_{-(\nu+1)}(\rho) - J_{\nu+2}(\rho)J_{-(\nu+2)}(\rho). \end{aligned}$$

From Eq. (1.17) we can express  $\rho$  as a function of  $L(\rho)$  and  $L'(\rho)$ , where the prime denotes the derivative with respect to  $\rho$ , and arrange the resulting expression as

$$\frac{\rho}{\nu} = 1 - \frac{1}{\nu} \frac{L(\rho, \nu)}{L'(\rho, \nu)}, \quad \text{or} \quad (1.18)$$

$$F(\rho, \nu) \equiv 1 - \frac{\rho}{\nu} - \frac{1}{\nu} \frac{L(\rho, \nu)}{L'(\rho, \nu)} = 0. \quad (1.19)$$

The first and second roots of Eq. (1.19),  $\rho_E$  and  $\rho_H$ , for a given value of  $\nu$ , correspond to the locations of the *elliptic* and *hyperbolic* points respectively.

The solution to Eq. (1.18) for a range of  $\nu$  is shown in Fig. 1.7, while the  $F(\rho, \nu)$  of Eq. (1.19) is plotted as a function of  $\rho/\nu$  for  $\nu \in [55.001, 55.999]$  in Fig. 1.8. It is now important to discuss the behavior of these solutions.

As we discussed above, we are only considering the cases with  $\nu \neq$  integer. Unfortunately, due to the asymptotic behavior of the Bessel function near the "turning point" [22], defined as  $\rho_{tp} = \sqrt{\nu(\nu+1)}$ , the solution approaches different limits as  $\nu$  gets close to an integer from different sides. This peculiar behavior is demonstrated for the case of  $\nu \sim 55$  in Fig. 1.8. Therefore, no simple analytical expression could be obtained for the position of the hyperbolic point. Instead, Fig. 1.7 shows a range of solutions for the location of this point. On the other hand, the elliptic point is very well defined. It is seen that for sufficiently large values of  $\nu$  the location of the elliptic point, according to our second-order perturbation analysis is at

$$\rho_E \simeq \frac{\nu}{2}, \quad \theta_E = \pi. \quad (1.20)$$

Although no simple expression could be found for the location of the hyperbolic point, we see from Fig. 1.7 that its location asymptotes (at large values of  $\nu$ ) to a value of  $\rho/\nu \sim (0.8 - 1.0)$ , therefore we may approximate

$$\rho_H \simeq 0.9\nu, \quad \theta_H = \pi. \quad (1.21)$$

It is also important to mention that because of the asymptotic behavior of Bessel functions, the elliptic and hyperbolic points could not always be found for small values of  $\nu$ . For these cases while the expression for the Hamiltonian, Eq. (1.16), is still valid, our analysis of the allowed and forbidden acceleration

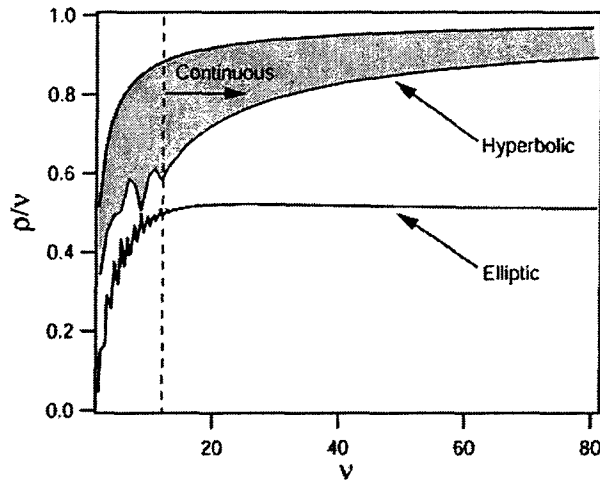


Figure 1.7: Solution to Eq. (1.18) as a function of  $\nu$ . The elliptic and hyperbolic points, **E** and **H**, could not always be found for small  $\nu$ . For  $\nu > 9$  both points could be found for any values of  $\nu$ . That region is marked as “continuous” on the figure.

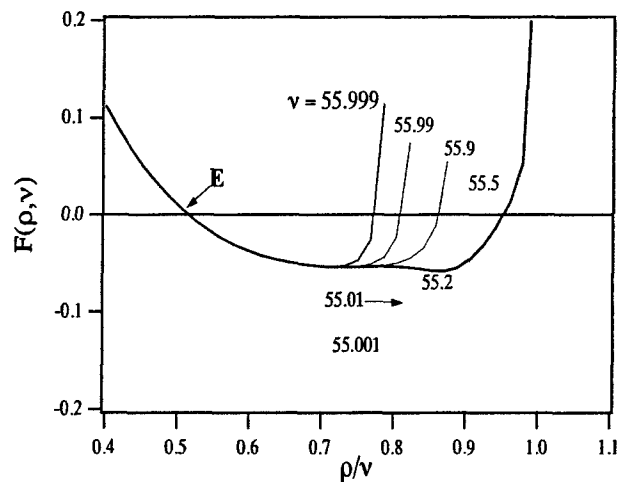


Figure 1.8: Plot of the function  $F(\rho, \nu)$ , given by Eq. (1.19), showing how the second root (corresponding to the hyperbolic point) moves away from  $\rho/\nu = 1$  as  $\nu$  changes from 55.001 to 55.999. The first root on the left, marked **E**, represents the elliptic point and the subsequent roots represent the hyperbolic points for the various values of  $\rho/\nu$ .

domains does not apply. The range of  $\nu$  for which we could always find both critical points is designated as "continuous" in Fig. 1.7.

Another limitation is placed on our analysis by its independence on  $\epsilon$  in locating the critical points, as seen from Eq. (1.17). Extensive numerical exploration of the weak dependence of the critical point locations on  $\epsilon$  suggests the following corrections to expressions (1.20) and (1.21), which are reminiscent of the  $\epsilon$  dependence in the single wave interaction [5], Eq. (1.7),

$$\rho_E \simeq \frac{(\nu - \sqrt{\epsilon})}{2}, \quad \theta_E = \pi, \quad (1.22)$$

$$\rho_H \simeq \nu - \sqrt{\epsilon}, \quad \theta_H = \pi. \quad (1.23)$$

The physical interpretation and significance of these two points could be understood as follows. Looking back at Fig. 1.1 we see that both points correspond to the particles moving  $180^\circ$  out of phase with the electric field of the wave. We can note from Fig. 1.6 that at the hyperbolic point the ion velocity is  $v_H = -\omega/k + v_{tr}$  and the Hamiltonian is at the maximum, while at the elliptic point the ion velocity is  $v_E = (-\omega/k + v_{tr})/2$ , and the Hamiltonian is at the minimum. The difference in the Hamiltonian of the two points then forms an "energy barrier", which an ion must overcome to be accelerated by the wave.

Another way to understand the importance of the elliptic point is to realize that at this point the energy exchange between the ion and the waves is minimum and the situation is equivalent to stable equilibrium for a pendulum. Any small perturbation from that equilibrium will only cause small oscillations about it. This implies that in the immediate neighborhood of point **E** the ion energy cannot be altered sufficiently to push the ion into the stochastic region, as seen in Fig. 1.5. On the other hand, the hyperbolic point corresponds to the unstable equilibrium of the pendulum and any small perturbation from it will cause significant changes in the ion motion, i.e. escape into the stochastic region and subsequent vigorous heating.

## 1.7 Beating Waves (On-Resonance)

When we choose  $\nu_i$  and  $\nu_j$  to be both on-resonance, the overall behavior becomes much more complicated and no simple analytical expression, as in the previous section, can be found. Fig. 1.9 shows a typical example, the case with  $\epsilon = 10$ ,  $\nu_i = 24$ , and  $\nu_j = 25$ . One of the major differences with respect to the off-resonance case is that now we have two hyperbolic points which do not lie at  $\theta = \pi$ . Nevertheless, we could still find their positions by solving equations (1.10) and (1.11) numerically.

The location of the elliptic point is easier to obtain since the first-order terms in Equations (1.10) and (1.11) drop out for  $\theta = \pi$ , as in the off-resonance case. Also, Fig. 1.9 shows that the analytical solution exhibits much more complicated chains of the critical points at large values of  $\rho$ . While in reality these points are "inside" the stochastic region, this graphical picture illustrates why the analytical treatment of the on-resonance case is more challenging. However, we

note that the locations of both the elliptic and the hyperbolic points even in this case are very close to those determined by Eqs. (1.6). Indeed, by studying numerically the solutions to Eq. (1.4) for both on-resonance and off-resonance cases we conclude that the locations of elliptic and hyperbolic points for both cases could be well predicted by Eqs. (1.6).

## 1.8 Summary and Concluding Remarks

The beating criterion ( $\omega_1 - \omega_2 = n\omega_c$ ) proposed by Benisti *et al.* [7, 8] can allow a magnetized ion to be energized by a pair of beating electrostatic waves. The importance of this mechanism stems from its ability to accelerate ions with arbitrarily low initial velocity. It has become clear however, (see Fig. 1.3) that this criterion is not sufficient for acceleration.

In order to better define the criteria for acceleration we investigated multiple ion trajectories (multiple initial conditions) on the same Poincaré cross-section. This analysis led to the identification of critical points on the phase diagram. Vigorous ion acceleration now can be explained in terms of the location of these points in the region of regular motion. A second-order perturbation analysis of the equation of motion allowed us to derive the criterion defining the allowed and forbidden acceleration domains in terms of the location of these points.

According to this analysis, for a pair of beating ( $\nu_1 - \nu_2 = 1$ ), electrostatic waves interacting nonlinearly with a magnetized ion, significant ion acceleration can occur as long as the Hamiltonian of the system *does not* satisfy the following "trapping" criterion

$$H_E < H(\rho_0; \theta_0) < H_H, \quad \text{with } \rho_0 < \nu - \sqrt{\epsilon}, \quad (1.24)$$

(which strictly applies when  $\nu \gg 1$ ). If the ion's initial conditions do not satisfy the above trapping criteria, the ion can be accelerated from arbitrarily low initial velocity through the region of regular motion to the stochastic region where substantial energization can occur.

Regular ion acceleration is a much slower process than stochastic energization [10]. However, as the wave amplitude is increased, the region of stochastic motion can extend down to low initial velocities. It is important to note that the trapping criterion is in terms of the (initial) *Hamiltonian* and not just the (initial) *velocity* ( $\rho_0$ ).

The necessary (wave-beating) condition stated in Eq. (1.8) along with the avoidance of the trapping criterion stated in Eq. (1.24) represent two *necessary and sufficient* conditions for the beating-wave ion acceleration mechanism to occur.

Finally, it is important to mention that the trapping criterion's independence of the wave energy  $\epsilon$  is a consequence of the second-order nature of the analysis. In light of the albeit weak dependence on  $\epsilon$  in the single-wave criterion in Eq. (1.7), we investigated numerically over a wide range of non-dimensional parameters ( $\epsilon \approx 5 - 100$ ,  $\nu \approx 10 - 50$ ) location of the critical points and found that

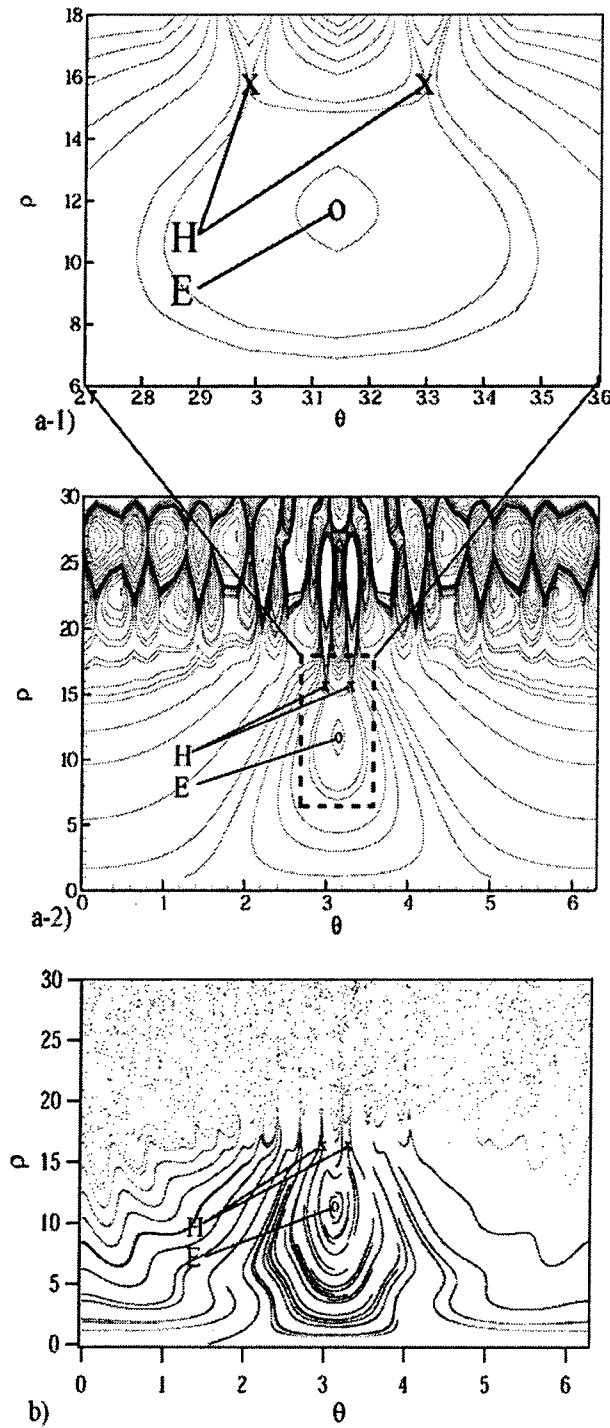


Figure 1.9: Poincaré cross-section for a particle interacting with two beating on-resonance waves showing a more complicated picture than that of the off-resonance case shown in Fig. 1.5. ( $\epsilon = 10$ ,  $\nu_i = 24$ ,  $\nu_j = 25$ ). a-1) and a-2) analytical solution. b) numerical solution.

the same dependence on applies. Therefore, given the locations of the critical points in Eq. (1.6) we can rewrite the trapping criterion in Eq. (1.24) as

$$\begin{aligned} H[(\nu - \sqrt{\epsilon})/2; \pi] &< H(\rho_0; \theta_0) < H(\nu - \sqrt{\epsilon}; \pi), \\ \text{with } \rho_0 &< \nu - \sqrt{\epsilon}. \end{aligned}$$

While the above study offers insight into the fundamental problem of a single ion interacting with two beating waves, the relevance of the mechanism to practical problems involving a plasma rests on resolving a number of issues: 1) the effects of oblique wave propagation, as recently studied in Ref.[23]; 2) the effects of wave dispersion; 3) the extension to collection of particles and the role of collisions. This last effect was a subject of numerical investigation in Ref.[21]. In that work we found that collisional scattering enhances ion energization by providing an escape mechanism for the ions trapped in the forbidden acceleration domain of phase space.

## 1.9 APPENDIX: $S_6^{\nu_i, \nu_j}(\rho)$ Term Simplification

Using Eq. (1.8) and substituting for  $J_m(\rho)$  and  $J'_m(\rho)$  with the following identities [22]

$$\begin{aligned} J_{m-1}(\rho) + J_{m+1}(\rho) &= \frac{2m}{\rho} J_m(\rho), \\ J_{m-1}(\rho) - J_{m+1}(\rho) &= J'_m(\rho), \end{aligned} \quad (\text{A-25})$$

we can rewrite  $S_6^{\nu_i, \nu_j}(\rho)$  as

$$\begin{aligned} S_6^{\nu_i, \nu_j}(\rho) &= \frac{1}{8} \left\{ \sum \frac{J_{m+2}(\rho) J_{m+1}(\rho)}{\nu - m} \right. \\ &+ \sum \frac{J_m(\rho) J_{m+1}(\rho)}{\nu - m} - \sum \frac{J_{m-1}(\rho) J_{m+2}(\rho)}{\nu - m} \\ &- \sum \frac{J_m(\rho) J_{m-1}(\rho)}{\nu - m} + \sum \frac{J_{m-1}(\rho) J_{m-2}(\rho)}{\nu - m} \\ &+ \sum \frac{J_{m+1}(\rho) J_{m-2}(\rho)}{\nu - m} - \sum \frac{J_m(\rho) J_{m-1}(\rho)}{\nu - m} \\ &\left. - \sum \frac{J_m(\rho) J_{m+1}(\rho)}{\nu - m} \right\}. \end{aligned} \quad (\text{A-26})$$

Now we use identity [24]

$$\sum_{m=-\infty}^{\infty} \frac{J_{m+p}(\rho) J_m(\rho)}{\nu - m} = \frac{\pi}{\sin \pi \nu} J_{p+\nu}(\rho) J_{-\nu}(\rho),$$

which is valid for  $p > 0$  to simplify Eq. (A-26) to

$$\begin{aligned} S_6^{\nu_i, \nu_j}(\rho) &= \frac{\pi}{8 \sin \pi \nu} [2J_{\nu+2}(\rho) J_{-(\nu+1)}(\rho) \\ &- 2J_{\nu}(\rho) J_{-(\nu-1)}(\rho)], \end{aligned}$$

which, with the help of identities (A-25), may be easily shown to equal to

$$S_6^{\nu_i, \nu_j}(\rho) = \frac{\rho}{\nu} \frac{\pi}{\sin \pi \nu} [J_{\nu+1}(\rho) J_{-(\nu+1)}(\rho) - J_{\nu-1}(\rho) J_{-(\nu-1)}(\rho)] + \frac{\rho}{(\nu+1)} \frac{\pi}{\sin \pi(\nu+1)} [J_{\nu}(\rho) J_{-\nu}(\rho) - J_{\nu+2}(\rho) J_{-(\nu+2)}(\rho)].$$

Chia *et al.* [13] showed that  $S_1^{\nu_i}(\rho)$  can be simplified as

$$S_1^{\nu_i}(\rho) = \frac{\pi}{8 \sin \pi \nu_i} [J_{\nu_i+1}(\rho) J_{-(\nu_i+1)}(\rho) - J_{\nu_i-1}(\rho) J_{-(\nu_i-1)}(\rho)].$$

It is then clear that

$$S_6^{\nu_i, \nu_j}(\rho) = \frac{\rho}{\nu_i} S_1^{\nu_i}(\rho) + \frac{\rho}{\nu_j} S_1^{\nu_j}(\rho). \quad (\text{A-27})$$

Finally, we caution that the relation (A-27) holds only for the special case of  $\nu_i \neq \text{integer}$  and  $\nu_j = \nu_i + 1$ .

## Chapter 2

# Effects of Ion Collisions on Ion Acceleration

### 2.1 Introduction

Acceleration of magnetized ions by beating electrostatic waves (BEW) is a non-linear phenomenon that may be occurring in nature and may have interesting applications to various problems including spacecraft propulsion. Observations made with the Topaz 3 rocket [9] indicated that ions are accelerated, in a region of natural electrostatic wave activity, in the topside ionosphere to the escape velocity. A puzzling issue is that initial velocities of these ions are significantly below the previously known threshold required for resonant acceleration by electrostatic waves. The threshold was derived in the context of ion interaction with a single electrostatic wave (SEW) [3, 5].

Benisti *et al.* [7, 8] proposed a non-resonant acceleration mechanism that relies on nonlinear interaction of an ion with a pair of beating waves. They showed that if the criterion

$$n\omega_c = \omega_2 - \omega_1, \tag{A-1}$$

is satisfied between any pair of electrostatic waves, ions can be accelerated from an arbitrary low initial velocity. Equation (A-1) states that the difference between the frequencies of the two beating waves  $\omega_1$  and  $\omega_2$  should equal to an integer multiple,  $n$ , of the ion cyclotron frequency  $\omega_c$ . This is in great contrast with the well known SEW-ion interaction studied theoretically by Karney *et al.* [3, 5], Zaslavsky *et al.* [24, 4], and Chia *et al.* [13, 20], and experimentally by Skiff *et al.* [6]. These studies showed that for acceleration to take place ion initial velocity has to be within a resonance band of the wave velocity. Another fundamental understanding obtained from these studies was that the ion motion during SEW-ion acceleration is always stochastic.

Choueiri and Spektor [10] investigated the beating wave acceleration mechanism theoretically and found that while Eq. (A-1) is *necessary* for the accel-

eration to occur, it is not a sufficient condition. Spektor and Choueiri [25] derived and verified the necessary *and* sufficient conditions for interaction, also discussed in section 2.2. When these conditions are satisfied, an ion with an arbitrary low initial velocity can accelerate through a regular (non-stochastic) motion in the electric field of the beating waves, then reach a threshold above which acceleration continues more vigorously (stochastically).

Since the BEW acceleration can increase the perpendicular velocity of *all* ions, as opposed to only the resonant part of the distribution function, it is of particular interest to spacecraft propulsion applications where acceleration or heating efficiency is of prime importance. In order to obtain the first indication of the existence of this mechanism we have designed and built a dedicated experiment using a helicon source and RF antenna to launch pairs of beating waves [26].

In order to guide the design of the experiment and help in interpreting its results we needed a model of the interaction that more resembles the case of a real plasma than does the single ion model. Such a model should account for the interaction of the waves with large amount of particles, and most importantly ion-ion collisions. In this study we present such a model based on using Monte Carlo techniques to describe collisions, and solving the equation of motion between collisions. We use the simulation to study parametrically the effects of ion collisions on the heating rate and attainable average energy for both SEW and BEW.

In section 2.2 we review the collisionless model that describes the interaction of a single particle with a spectrum of electrostatic waves. We also review previous findings resulting from that model. In section 2.3 we present the numerical model that allows tracking a large number of ions and account for a finite collision rate. In section 2.4 we present and discuss the results of our numerical investigation, and in section 3.7 we summarize our findings and deduce a phenomenological picture that illustrates the fundamental differences between BEW and SEW ion acceleration.

## 2.2 Single Particle Model

A theoretical model for beating electrostatic waves interacting with a single ion is given in [7, 8, 25]. The description, which latter in this chapter is augmented with inclusion of collisions and the ability of tracking many ions, is shown schematically in Fig. 2.2. The schematic shows an ion in a constant magnetic field  $B\hat{z}$  and electrostatic wave traveling in transverse direction  $\hat{x}$ . The wave interacts with a gyrating ion causing a change in its Larmor radius. Because the magnetic field is constant, an increase in the Larmor radius directly corresponds to the increase in the ion's perpendicular velocity and thus its kinetic energy. The equation of motion governing the interaction between a spectrum of propagating electrostatic waves and a single ion can be easily

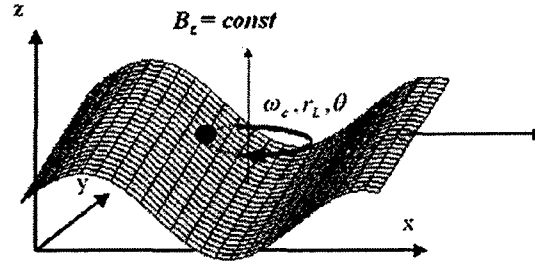


Figure 2.1: A single ion of charge  $q$  and mass  $m$  in a constant homogeneous magnetic field  $B\hat{z}$  interacts with an electrostatic wave. The wavenumber and electric field of the wave is parallel to the  $x$ -axis.

derived [3, 13]:

$$\frac{d^2x}{dt^2} + \omega_c^2 x = \frac{q}{m} \sum_i E_i \sin(k_i x - \omega_i t + \phi_i), \quad (\text{A-2})$$

where  $x$  and  $t$  are the coordinate and the time variables,  $q$  and  $m$  are the charge and the mass of the ion,  $\omega_c = qB/m$ ,  $E_i$ ,  $k_i$ ,  $\omega_i$ , and  $\phi_i$  are the amplitude, wave number, frequency and phase of the  $i^{\text{th}}$  electrostatic wave. While Fig. 2.2 shows a single wave, a similar picture can be drawn for a spectrum of electrostatic waves traveling in the same direction. It is convenient to normalize the above equation and express it in the canonical form [14, 12]:

$$H = \rho^2/2 + \sum_i \frac{\varepsilon_i}{\kappa_i} \cos(\kappa_i \rho \sin \theta - \nu_i \tau + \varphi_i), \quad (\text{A-3})$$

where  $H$  is the Hamiltonian of the system,  $\kappa_i = k_i/k_1$ ,  $\nu_i = \omega_i/\omega_c$ ,  $\tau = \omega_c t$ ,  $\varepsilon_i = (k_1 q E_i)/(m \omega_c^2)$ ,  $\rho^2 = X^2 + \dot{X}^2$ , and  $X = k_1 x$ ,  $\dot{X} = dX/d\tau$ , so that  $X = \rho \sin \theta$ ,  $\dot{X} = \rho \cos \theta$ . Where  $\theta$  is the cyclotron rotation angle measured clockwise from the  $y$ -axis as shown in Fig. 2.1, and  $\rho$  is the normalized Larmor radius. Equations (A-2) and (A-3) could be solved numerically with either conventional 4<sup>th</sup> order Runge-Kutta scheme or a symplectic approach. We have used the symplectic integration method developed by Candy and Rozmus [17] to study the behavior of a single ion interacting with one or two propagating electrostatic waves.

We were able to confirm [25] that while a single electrostatic wave produces some ion heating under restricted (resonance) conditions, two beating waves can result in ion acceleration from arbitrary low initial velocities. We have also shown that Eq. (A-1) describes the *necessary*, but not *sufficient* condition for that heating to take place. The necessary and sufficient conditions for ion heating by the beating electrostatic waves are [25]:

$$n\omega_c = \omega_2 - \omega_1, \quad (\text{A-4})$$

$$H(\rho; \theta) = H_H > H(\rho \simeq \nu - \sqrt{\varepsilon}; \theta = \pi), \quad (\text{A-5})$$

where  $H_H$  is the value of the Hamiltonian evaluated at the hyperbolic point as described in Ref.[25] and shown schematically in Fig. 2.2.

The schematic shows the possible acceleration processes. Particle 1 is accelerated stochastically in both cases. Particle 2 with initial energy below the SEW resonance threshold ( $\rho = \nu - \sqrt{\epsilon}$ ) is affected by BEW but is never allowed to reach the stochastic region. While particle 3 remains unaffected by the SEW interaction, it can be effectively accelerated by BEW through regular (non-stochastic) motion that allows it to reach stochastic region, where more rigorous acceleration takes place.

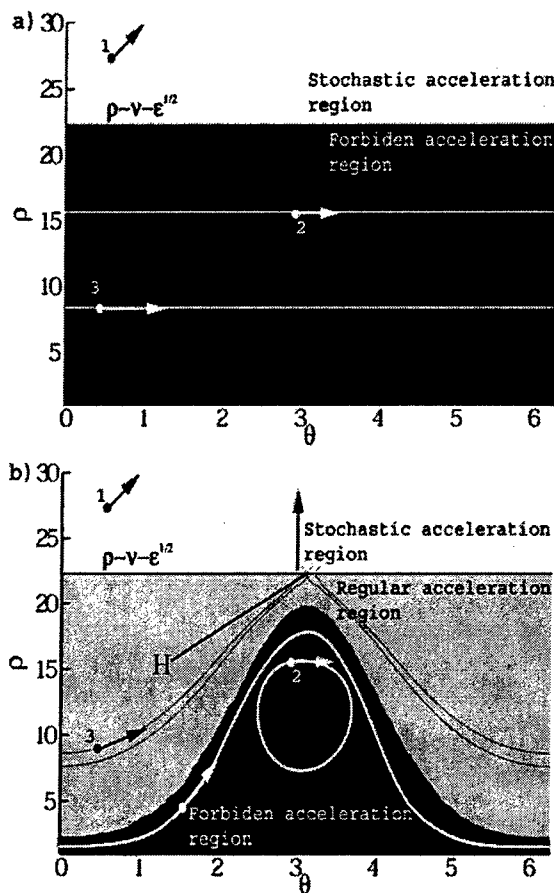


Figure 2.2: Poincaré cross-section (phase diagram) schematic. The figure shows typical trajectories for various initial conditions of ion interacting with: a) a single electrostatic wave (SEW), b) beating electrostatic waves (BEW).

## 2.3 Including Collisions

Collisions alter the picture described in the previous section drastically. Without collisions an ion whose initial velocity (Hamiltonian) is below that corresponding to Eq. (A-5), particle 2 in figure 2.2b will never be effectively accelerated by the waves. However, a collision would instantaneously change that ion's trajectory and place it in a part of phase space where Eq. (A-5) is satisfied.

In this section we consider ion collisions only. Coulomb ion collisions are of interest since they thermalize the heavy species energy and since our main focus is ion heating.

To introduce collisions into our numerical model we follow the classical work of Takizuka and Abe [27]. We model Coulomb collisions as small angle binary collisions and assume that on a sufficiently small time scale we can uncouple particle motion from collisions. Thus our algorithm consists of two parts. We move all particles between collisions according to the equation of motion prescribed by the single particle collisionless model, Eq. (A-2). We then use the Monte Carlo approach to determine randomly the collision partners and the scattering angles for each collision.

### 2.3.1 Overall implementation

1. We first choose a time step  $\Delta t$  smaller than the ion-ion relaxation time calculated at the initial temperature of the ions.
2. Using a 4<sup>th</sup> order Runge-Kutta scheme we then follow each particle in our simulation for  $\Delta t$  seconds according to the equation of motion for a single ion, Eq. (A-19).
3. Next we randomly choose a collision partner for each ion.
4. Using Monte Carlo method we then determine the velocity increments for all colliding pairs as described in section 2.3.2. The new velocities are fed back into the Runge-Kutta solver.
5. After each collision, we store the value of the scattering angle  $\Theta$  for each particle. We assume that whenever  $\sum \sin^2 \Theta \geq 1$  the particle has undergone one ion-ion Coulomb collision. Here the summation is over successive collisions for a given particle.

### 2.3.2 Momentum exchange during a collision

We treat Coulomb collisions between ions as a small angle binary elastic scattering events [27]. Such collisions preserve energy and momentum.

The relative velocity vector  $\mathbf{u}(u_x, u_y, u_z)$  for a colliding pair is:

$$\mathbf{u} = \mathbf{v}_a - \mathbf{v}_b, \quad (\text{A-6})$$

where  $\mathbf{v}_a$  and  $\mathbf{v}_b$  are the velocities of two colliding ions. The post-collision relative velocity  $\mathbf{u}^f$  is:

$$\mathbf{u}^f = \mathbf{u}^i + \Delta\mathbf{u}, \quad (\text{A-7})$$

where  $\mathbf{u}^i$  is the relative velocity right before the collision and  $\Delta\mathbf{u}$  is the change in the relative velocity due to the collision. The change in the relative velocity due to a scattering event could be derived from conservation principles [27],

$$\begin{aligned} \Delta u_x &= (u_x/u_\perp)u_z \sin \Theta \cos \Phi - (u_y/u_\perp)u \sin \Theta \sin \Phi \\ &\quad - u_x(1 - \cos \Theta), \end{aligned} \quad (\text{A-8})$$

$$\begin{aligned} \Delta u_y &= (u_y/u_\perp)u_z \sin \Theta \cos \Phi + (u_x/u_\perp)u \sin \Theta \sin \Phi \\ &\quad - u_y(1 - \cos \Theta), \end{aligned} \quad (\text{A-9})$$

$$\Delta u_z = -u_\perp \sin \Theta \cos \Phi - u_x(1 - \cos \Theta), \quad (\text{A-10})$$

where  $u_\perp^2 = u_x^2 + u_y^2$  and  $u^2 = u_\perp^2 + u_z^2$ . Here perpendicular and parallel directions are defined relative to the magnetic field ( $\hat{z}$ -axis). When  $u_\perp = 0$  we have,

$$\Delta u_x = u \sin \Theta \cos \Phi, \quad (\text{A-11})$$

$$\Delta u_y = u \sin \Theta \sin \Phi, \quad (\text{A-12})$$

$$\Delta u_z = -u(1 - \cos \Theta). \quad (\text{A-13})$$

Angle  $\Phi$  is chosen homogeneously randomly from 0 to  $2\pi$ . Angle  $\Theta$  is chosen according to:

$$\sin \Theta = \frac{2\delta}{1 + \delta^2}, \quad (\text{A-14})$$

$$1 - \cos \Theta = \frac{2\delta^2}{1 + \delta^2}, \quad (\text{A-15})$$

where  $\delta = \tan(\Theta/2)$  is a random number chosen with the Gaussian distribution centered around zero and having the following variance  $\langle \delta^2 \rangle$ :

$$\langle \delta^2 \rangle = \Delta t \frac{q^4 n \lambda}{\pi \epsilon_0^2 m^2 \|\mathbf{u}\|^3}, \quad (\text{A-16})$$

where  $q$  and  $m$  are the charge and the mass of the ion,  $n$  is the particle number density,  $\lambda$  is the Coulomb logarithm,  $\epsilon_0$  is the permittivity of free space,  $\|\mathbf{u}\|$  is relative speed of two colliding ions, and  $\Delta t$  is the time step [27]. This small angle restriction allows us to interpret as the ion-ion collision frequency  $\nu_{ii}$  to the binary collision frequency  $\nu_b$  and the formalism implicitly accounts for electron shielding. We did not however track the electron dynamics as electrons are not expected to be effected by low frequency of the wave. We assume that the electron temperature is not affected by the low frequency waves of the problem,  $\omega < \omega_{ce}$ .

The post-collision velocity of each particle is found simply from,

$$\mathbf{v}_a^f = \mathbf{v}_a^i + (m/2)\Delta\mathbf{u}, \quad (\text{A-17})$$

$$\mathbf{v}_b^f = \mathbf{v}_b^i + (m/2)\Delta\mathbf{u}. \quad (\text{A-18})$$

### 2.3.3 Moving the particles

Starting from the Lorentz force equation,

$$\mathbf{F} = m\ddot{\mathbf{x}} = q(\mathbf{E} + \mathbf{v} \times \mathbf{B}), \quad (\text{A-19})$$

we can derive equations of motion for a single particle in three dimensions. In our analysis, the magnetic field is constant,  $\mathbf{B} = B\hat{z}$ , and the electric field arises from the propagating electrostatic waves, as shown in Fig. 2.1,

$$\ddot{x} = \dot{y} + E \sum_i \sin(x - \omega_i t), \quad (\text{A-20})$$

$$\ddot{y} = -\dot{x}, \quad (\text{A-21})$$

$$\ddot{z} = 0, \quad (\text{A-22})$$

so that  $\ddot{x}$ ,  $\ddot{y}$ , and  $\ddot{z}$  are the second derivatives with respect to time  $t$ , and the other variables are the same as those appearing in equations (A-2) and (A-3). Equations (2.3.3) could be solved numerically using 4<sup>th</sup> order Runge-Kutta method.

## 2.4 Simulation

The above model is used to simulate the case of BEW acceleration ( $\varepsilon = 10$ ,  $\nu_1 = 24.3$ ,  $\nu_2 = 25.3$ ,  $\kappa_i = 1$ ) and compared to those of SEW acceleration under similar condition ( $\varepsilon = 10$ ,  $\nu = 24.3$ ). To visualize the numerical results we use Poincare cross-sections ( $\rho$  vs.  $\theta$  phase diagrams) [12]. We will also investigate how collisions influence the energy evolution of the entire system.

### 2.4.1 Phase diagrams

Figure 2.3 follows collisionless evolution of 1000 particles in the plot  $\rho$  vs.  $\theta$ . Initially we distribute all particles homogeneously over region of the phase space  $\rho \leq 20$ . The stochastic heating is observed whenever ions reach the *stochastic* zone ( $\rho > 20$ ), Fig. 2.2b. Particles with initial conditions lying outside prohibited zone are accelerated as could be seen from that figure. The points corresponding to unaccelerated particles define a mount-like structure, seen in the last two panels of Fig. 2.3, which corresponds to prohibited zone shown in figure 2.2b. Figure 2.4 shows the BEW ion acceleration case where the evolution of phase space points is qualitatively different than the collisionless case illustrated in 2.3. Even ions originally in the forbidden acceleration zone are accelerated.

### 2.4.2 Energy Evolution

Now that we showed that collisions enhance ion heating, we will analyze the energy evolution of the entire system. In this section we compare the cases of BEW and SEW ion acceleration by beating electrostatic waves and a single electrostatic wave.

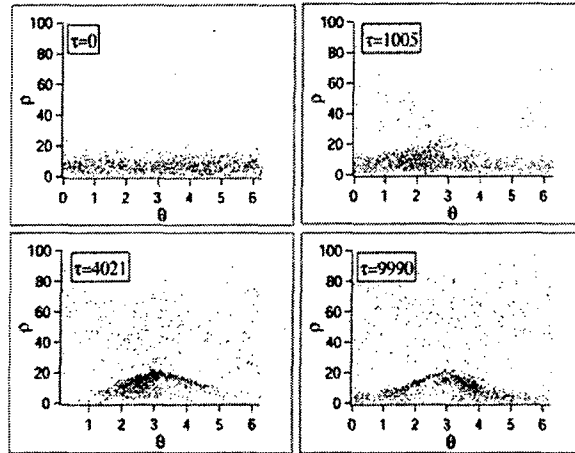


Figure 2.3:  $\varepsilon = 10$ ,  $\nu_1 = 24.3$ ,  $\nu_2 = 25.3$ . Collisionless case. The "hump" corresponds to the particles not accelerated by the beating waves in accordance with Eq. (2.2).

Figure 2.5 shows perpendicular component of the energy for BEW as well as SEW cases. Initially the energy increases exponentially. This corresponds to ions funnelling to the stochastic region. The process is analogous to phase space diffusion - thus its exponential nature. As more particles find their way into the stochastic region, the exponential increase is followed by the equilibration of the energy (by stochastic motion and collisions). Because particles fill up the stochastic region randomly, the statistical average of the energy stays constant.

Figure 2.5 demonstrates that collisions significantly increase both the ion heating rate and the final average energy.

In order to help us further illustrate these effects better we have ran the simulation with the collision frequency restrained to a constant value irrespective of the temperature. Figure 2.6 shows the results for four such cases and a simulation with self-consistent collision frequency calculation, for comparison. The figure indicates that there is an optimum collision frequency at which the heating rate and efficiency are at the maximum. When the collision frequency is increased from 0 to  $\nu_b = 0.04\omega_c$ , the ions diffuse faster into the stochastic region and the heating efficiency improves. However, as the collision frequency is further increased ( $\nu_b = 4.14\omega_c$ ), the heating rate as well as the efficiency start dropping because collisions increasingly disturb ion motion too much. In a real plasma the ion collision frequency scales as  $\sim T_{ion}^{-3/2}$  (for  $T_i \leq T_e$ ). As the electrostatic waves deposit their energy into the plasma, the ions collide less often and the collision frequency drops to its optimum value. However, if the collision frequency decreases even further, the heating efficiency drops, driving down the temperature and stabilizing the collision frequency back to its optimum value. Therefore, we can conclude that the collision frequency always changes to ac-

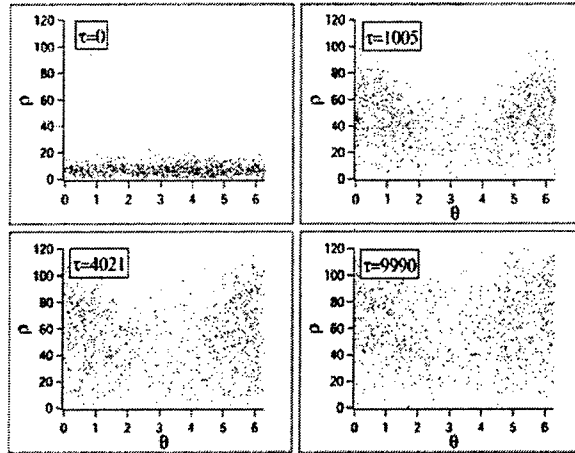


Figure 2.4:  $\varepsilon = 10$ ,  $\nu_1 = 24.3$ ,  $\nu_2 = 25.3$ . Particles are allowed to collide with each other. We take the initial collision frequency required for step 1 of our algorithm to be  $\sim 10^6$ , which corresponds to  $n_e \sim 10^{12} \text{ cm}^{-3}$  and  $T_e = 300 \text{ K}$ . Unlike Fig. 2.3, beating electrostatic waves accelerate all ions.

commodate the maximum possible heating rate. This becomes more evident by comparing the clamped value of  $\nu_b$  simulations (dashed lines) to the solid line which was obtained by running the simulation and allowing the collision frequency to change self-consistently with the ion temperature evolution.

## 2.5 Conclusions

Numerical simulations of the nonlinear interaction of magnetized ions with beating electrostatic waves (BEW) were carried out. The resulting particle heating was compared to that obtained from simulations with interaction with SEW under the same conditions. The higher heating rate and temperature attained in BEW acceleration can be explained through the following fundamental description. In the SEW interaction thermalizing collisions are the only means for particles below a certain threshold of energy, associated with the resonant condition, to reach the region of phase space where stochastic and vigorous heating takes place. The non-resonant character of BEW acceleration allows a significant fraction of the ion distribution function to be accelerated and reach the stochastic region. This acceleration is augmented by collisions. In addition to the thermalizing role of collisions, this simulation-supported phenomenological picture points to the promise of using BEW as a new and efficient method for accelerating magnetized ions in a real plasma.

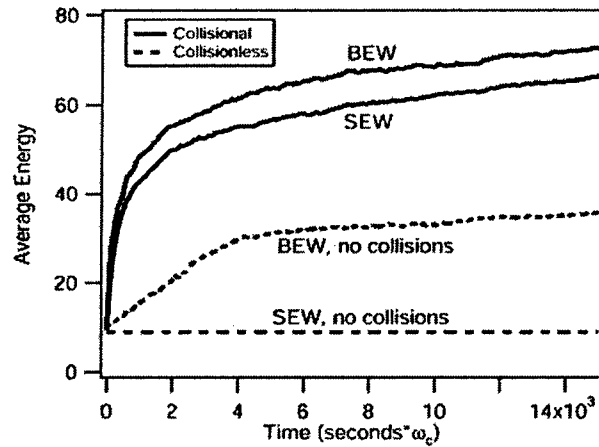


Figure 2.5: Perpendicular energy evolution for 1000 particles interacting with beating waves.  $\epsilon = 10$ ,  $\nu_1 = 24.3$ ,  $\nu_2 = 25.3$ . For comparison we also show the energy evolution for the single wave-ion interaction.  $\epsilon = 10$ ,  $\nu = 24.3$ .

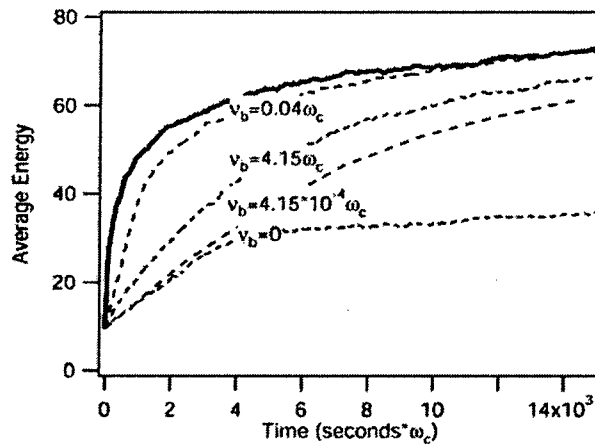


Figure 2.6: Perpendicular energy evolution for 1000 particles interacting with beating waves. Dashed lines correspond to the clamped values of collision frequency and solid curve represents the self-consistent simulation.  $\epsilon = 10$ ,  $\nu_1 = 24.3$ ,  $\nu_2 = 25.3$ .

## Chapter 3

# Beating Waves Experiment: Excitation of Ion Cyclotron Waves and Demonstration of Ion Acceleration

### 3.1 Introduction

Inductive rf plasma sources, and in particular helicon plasma discharges, are of interest in propulsion research because of their high plasma production efficiency and controllability [28, 29]. Unfortunately, these rf plasma sources produce cold ( $T_i \sim 0.1$  eV) ions. To achieve high  $I_{sp}$  it is thus necessary to heat these ions considerably.

Various types of electrodeless plasma heating (ion acceleration) provide an efficient way to increase ion temperature. Methods such as the Ion Cyclotron Range Heating (ICRH), Lower Hybrid (LH) wave heating, and the current drive have been suggested for ion heating in fusion devices [30, 31, 32]. The ICRH scheme is also employed in the VASIMR experimental rocket concept [33, 34, 35]. In addition, ion heating by various electromagnetic and electrostatic instabilities has been observed in the Earth ionosphere [36, 37, 38, 39, 40].

In this chapter we investigate excitation of Electrostatic Ion Cyclotron (EIC) waves that propagate transversely to the external magnetic field. Our previous theoretical and numerical studies have shown that two beating electrostatic waves, obeying specific criteria [10, 25, 41, 42], may energize ions very efficiently. Such ion energization mechanism can prove to be useful in propulsion applications.

There is a lack of detailed measurements of EIC wave properties and propagation in rf-sustained plasmas. It is with this goal in mind that we investigate the excitation and propagation of EIC waves across a magnetized rf-sustained

plasma column, and subsequent ion energization by these waves. In the above sections we have not dealt with ion energization but focused on the excitation and propagation of EIC waves. The energization is demonstrated in the last section.

This chapter is organized as follows. In section 3.2 we review previous experimental work on electrostatic wave launching. Then in section 3.3 and 3.4 we describe our experimental apparatus and the diagnostics used to detect and study the waves. In section 3.5 we analyze the electrostatic waves launched in our apparatus. We summarize our results regarding wave excitation in section 3.7. We finally conclude in the last section with the experimental demonstration of the existence of the new ion acceleration mechanism.

## 3.2 Review of previous work

Various experiments reported on vigorous ion energization by EIC waves in magnetized plasmas. However, most of these studies relied on exciting EIC waves through some internal plasma instability. Two typical experimental configurations are shown in Fig. 3.1.

In these experiments an electrostatic wave of frequency  $\sim \omega_{ci}$  is excited either by drawing electron current along the magnetic field to a positively biased small electrode, as shown in Fig. 3.1a, or by creating an electric field perpendicular to the external magnetic field, as shown in Fig. 3.1b. In both cases significant ion energization was observed once the wave was excited [44, 45]. Unfortunately in experiments like these, it is impossible to separate the cause from the effect - the ion energization from the wave generation mechanism. In addition the wave frequency cannot be controlled. Thus to investigate ion energization properly one needs to design an experiment where the waves are excited by some externally controlled antenna.

Four such antenna configurations are shown in Fig. 3.2. Hooke and Barnabei [46] used capacitively coupled plates, shown in Fig. 3.2a, and Stenzel and Gekelman [47] employed a set of wires strung along the magnetic field, as shown in Fig. 3.2b, to launch waves close to the LH resonance. Schmitt launched Pure Ion Bernstein Waves (PIBW) with a single wire at the center of the plasma column [48], Fig. 3.2c, while Schmitt and Krumm launched Bernstein waves through a mode conversion mechanism with a wire coil wrapped around the plasma column [49], Fig. 3.2d.

Goree *et al.* [50] and Skiff *et al.* [6] used electrostatic plate antenna to launch a *single* electrostatic wave above the ion cyclotron frequency transversely to the magnetic field. Significant stochastic ion energization was reported in the latter experiment. Since our theoretical and numerical investigations have focused on similar frequency range we have adopted this antenna design for our experiment.

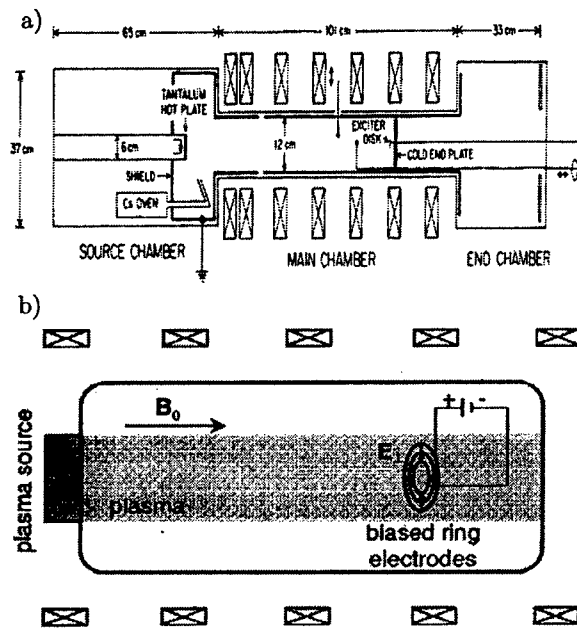


Figure 3.1: Typical setup for studying Electrostatic Ion Cyclotron (EIC) wave. a) Used by Motley and D'Angelo [43] to excite current driven EIC. The picture is taken from Ref. [44]. b) Used by Koepke *et al.* to excite inhomogeneous energy density driven EIC. The picture is taken from Ref. [45].

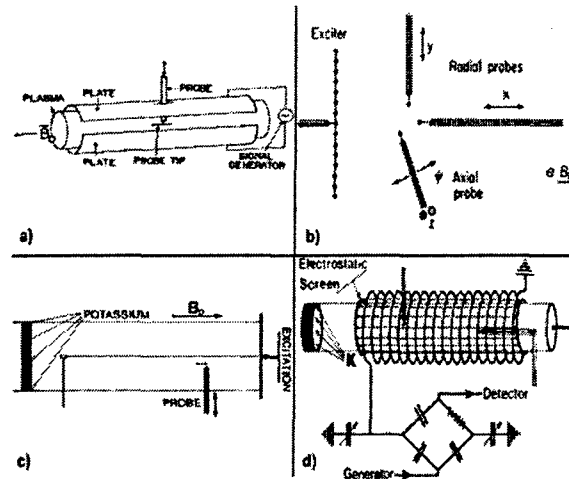


Figure 3.2: Various antenna designs for launching waves into a plasma. a) Capacitively coupled plates, and b) a set of wires strung along the magnetic field launch waves close to the LH resonance. c) A single wire at the center of the plasma column, and d) a coil wrapped around the plasma column launch Bernstein waves.

### 3.3 Experimental setup

#### 3.3.1 Vacuum Chamber

A schematic of the Beating Wave experimental apparatus (BWX) is shown in Fig. 3.3. It consists of two pyrex cylinders placed inside a 0.1 Tesla magnet. The axial magnetic field along the centerline is shown in Fig. 3.4. The two curves correspond to the ion cyclotron frequency of 10 kHz and 30 kHz in the test section of the vacuum chamber. The small cylinder is 6 cm in diameter (ID) and 37 cm in length while the large cylinder is 20 cm in diameter (ID) and 46 cm in length. The backplate of the small cylinder is made from molybdenum and is electrically floating to minimize sputtering. The two cylinders are connected by an electrically floating aluminum plate with a 6 cm concentric hole at the center to allow free flow of gas between the cylinders. A uniform fill pressure of 1 to 30 mTorr is maintained by a gas feed (Ar or He) at the aluminum endplate of the large cylinder and by a 150 l/s turbo pump with a conductance controller backed up by a roughing pump. The system is capable of maintaining a base pressure of  $2 \cdot 10^{-6}$  Torr.

Once the plasma discharge is ignited in the small cylinder, the plasma propagates along the magnetic field lines, which are parallel to the axis of the cylinders, into the large chamber where the wave-launching and plasma-energization experiments are conducted.

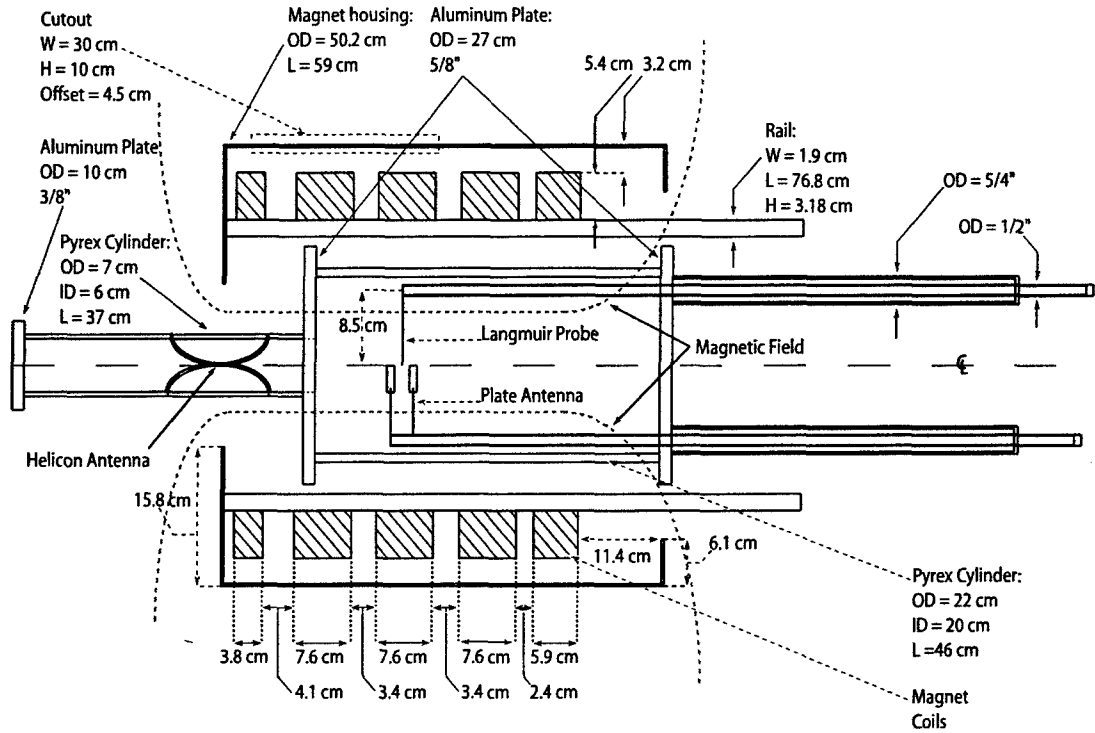


Figure 3.3: The drawing of the BWX experimental apparatus.

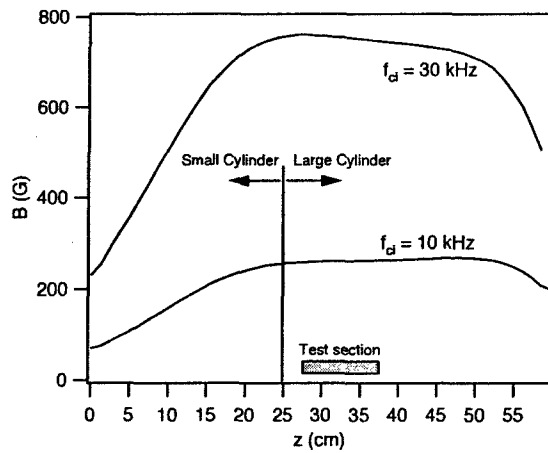


Figure 3.4: The axial magnetic field ( $B_z$ ) along the centerline of the magnet. The ion cyclotron frequency is relatively constant within the test portion of the large chamber where the electrostatic waves are launched.

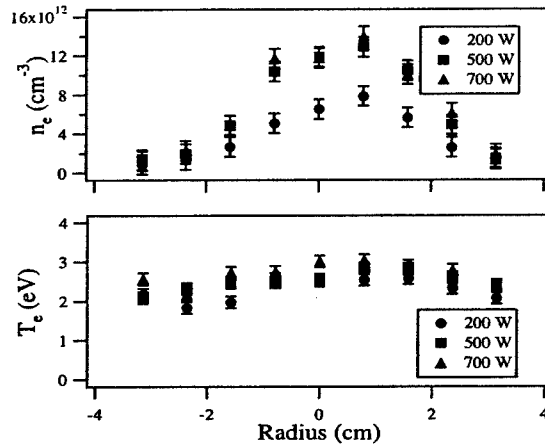


Figure 3.5: Plasma density and electron temperature for various rf power to the saddle antenna. As rf power is raised above 500 W the high plasma density helicon discharge is observed.  $B=782$  Gauss,  $P=1\text{mTorr}$ .

### 3.3.2 Plasma Source

A Boswell saddle type antenna used to create the plasma discharge is placed around the small cylinder. The antenna is made of 0.25" copper tubing to allow water cooling. An inductive discharge is produced by supplying rf power to the antenna from an ENI 13.56 MHz 1.2 kW power supply through a tuner. The tuner consists of an L network made of two Jennings 1000 pF 3 kV variable vacuum capacitors. The tuner is placed as close to the antenna as possible to maximize coupling.

An inductive discharge is easily obtained with only a few watts of forward rf power to the antenna and only a few percent of rf power reflected. A helicon discharge with high plasma density ( $10^{13} \text{ cm}^{-3}$ ) can be produced as rf power to the antenna is raised above 500 W by properly adjusting the pressure and magnetic field. The inductively coupled discharge looks homogeneous and occupies the entire cross-section of the small cylinder. When the helicon discharge is obtained with argon, a bright blue column is observed at the centerline. Measured radial distributions of plasma density and electron temperature for both types of the discharges are shown in Fig. 3.5. Figure 3.6 shows the range of some natural plasma frequencies that were calculated with measured  $T_e$ ,  $n_e$ , and  $B$ .

### 3.3.3 Beating Waves Antenna

In attempt to launch electrostatic waves into the plasma column we have tried a couple of antenna configurations. An external antenna consisting of two spools of wire in the Helmholtz coil configuration, placed on opposite sides of the out-

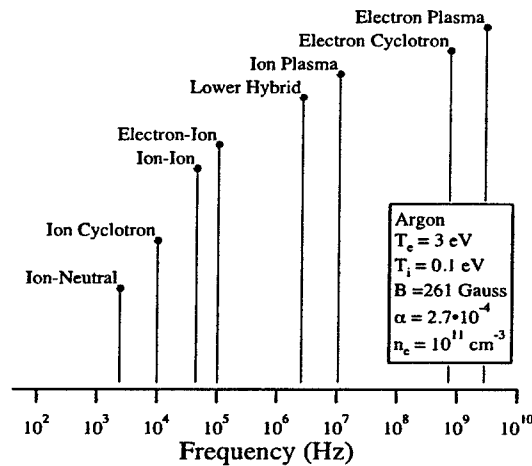


Figure 3.6: Typical plasma parameters for the BWX experiment calculated with measured  $T_e$ ,  $n_e$ .

side wall of the vessel, with their axis perpendicular to the magnetic field were initially used but did not excite electrostatic waves. The hope was that electromagnetic waves from this external antenna could be converted into electrostatic waves by the plasma [51, 52]. We were able to launch an electrostatic wave with an antenna placed inside the vacuum chamber, and consisting of two flat metal plates. This type of antenna has been used to launch a single electrostatic wave above the ion cyclotron frequency by Goree *et al.* in the toroidal ACT-1 device [50, 53], and by Skiff *et al.* in a linear device [6]. The antenna is made of two 1 cm  $\times$  6 cm molybdenum plates placed 3.14 cm apart along the magnetic field. The plates are oriented such that the long side and the surface normal are perpendicular to the magnetic field, as shown in Fig. 3.3. During the wave-launching experiments reported below, the plates were driven by a Wavetek 180 signal generator with a sinusoidal signal through a Tektronix AM 501 modular op-amp either in or out of phase, as shown in Fig. 3.7.

### 3.4 Diagnostics

Two types of Langmuir probes were employed to measure the steady-state plasma properties and the wave propagation. Plasma density and electron temperature were determined using a radio frequency compensated Langmuir probe with 0.5 mm graphite tip [54]. The rf compensation was achieved with four miniature inductors placed in series and close to the probe tip. The inductors were chosen to filter out the fundamental at 13.56 MHz and the second harmonic at 27.12 MHz of the helicon antenna signal. Uncompensated Langmuir probes with either graphite or T-shaped tips made of 10 mil tungsten wire were

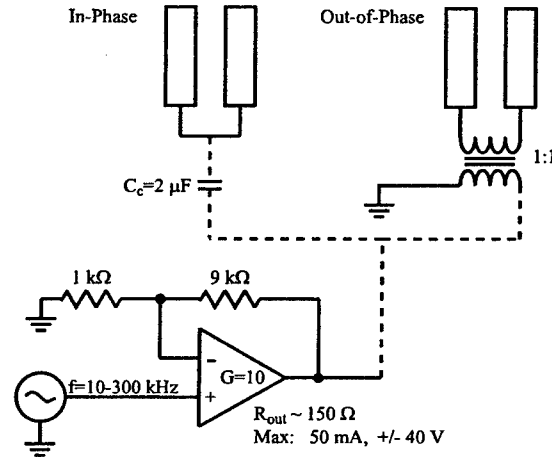


Figure 3.7: The circuit diagram for launching a single electrostatic wave into the plasma column. The two antenna plates can be driven in or out of phase.

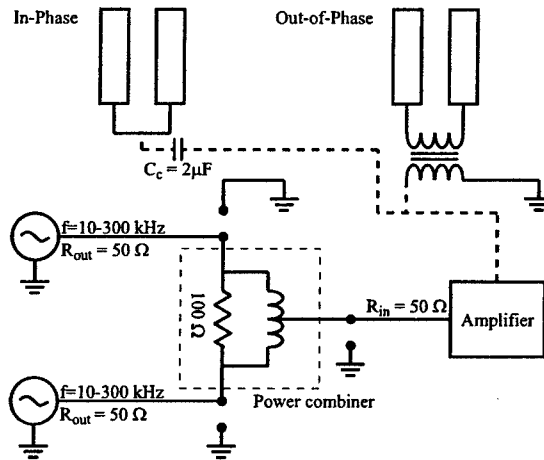


Figure 3.8: To launch a pair of beating waves the impedance between the two signal sources and the amplifier has to be matched through a power combiner.

used to detect the wave and investigate its dispersion.

Instead of the Laframboise analysis [55] of the Langmuir probe I-V characteristic we used an empirical floating potential method specifically developed by Chen *et al.* [56] to determine  $T_e$  and  $n_e$  with rf-compensated Langmuir probes in helicon-sustained plasmas similar to ours.

### 3.5 Wave launching

The circuit used to launch a single electrostatic wave into the plasma column is shown in Fig. 3.7. The sinusoidal signal (10-300 kHz) from a Wavetek 180 signal generator is amplified with gain of 10 by a Tektronix AM 501 modular operational amplifier ( $R_{out} \sim 150 \Omega$ ,  $\pm 40$  V, 50 mA Max.). To drive the plates in phase the signal is sent to both plates. A coupling capacitor ( $C_c = 2 \mu F$ ) can be used, as indicated in Fig. 3.7, to allow both plates to float with respect to the plasma potential. To drive the plates out of phase the antenna is connected through a 1:1 transformer.

The launching of a pair of beating waves into the plasma is accomplished by combining the output from two signal sources. This is achieved by mixing the low-power signals coming out from two Wavetek signal generators and sending the combined output to an amplifier, as demonstrated in Fig. 3.8. The output impedance of the signal generators and the input impedance of the amplifier is  $50 \Omega$ . To make sure that the signal of one of the signal generators is not distorted by the other, we needed to match the impedance of the entire circuit. A power combiner consisting of a  $100 \Omega$  resistor and a tapped inductor in parallel provide good matching between the signal generators and the amplifier.

To ensure that the waves are launched into the plasma efficiently we also needed to maintain a good antenna-plasma coupling. Different amount of power is delivered to the antenna plates depending on the impedance mismatch between the driving antenna circuit and the plasma. Plasma impedance varies with the plasma density, i.e. with rf power delivered to the helicon antenna, and the fill-up pressure. For a given pressure the power to the antenna plates and the efficiency of the electrostatic wave launching can be correlated to the helicon antenna power.

In order to investigate the wave launching conditions we conducted the following experiment. The signal generator and the op-amp in Fig. 3.7 were set to produce a 30-Volt sinusoidal signal ( $\omega = 70$  kHz) with no plasma. A magnetized argon plasma with  $n_e = 10^9 - 10^{13} \text{ cm}^{-3}$  and  $f_{ci} = 30$  kHz was produced by the helicon antenna with the chamber back filled to 1 mTorr. Measuring the plates voltage and current simultaneously we were able to determine the impedance and the power delivered to the antenna plates as a function of rf power delivered to the helicon antenna. A Langmuir probe inserted into the plasma column measured the amplitude of the launched waves.

We found that for the in-phase configuration the maximum power to the antenna plates is delivered when rf power is 175-200 W, as shown in Fig. 3.9a and 3.9b. The amplitude of the Langmuir probe signal is a complicated function of rf

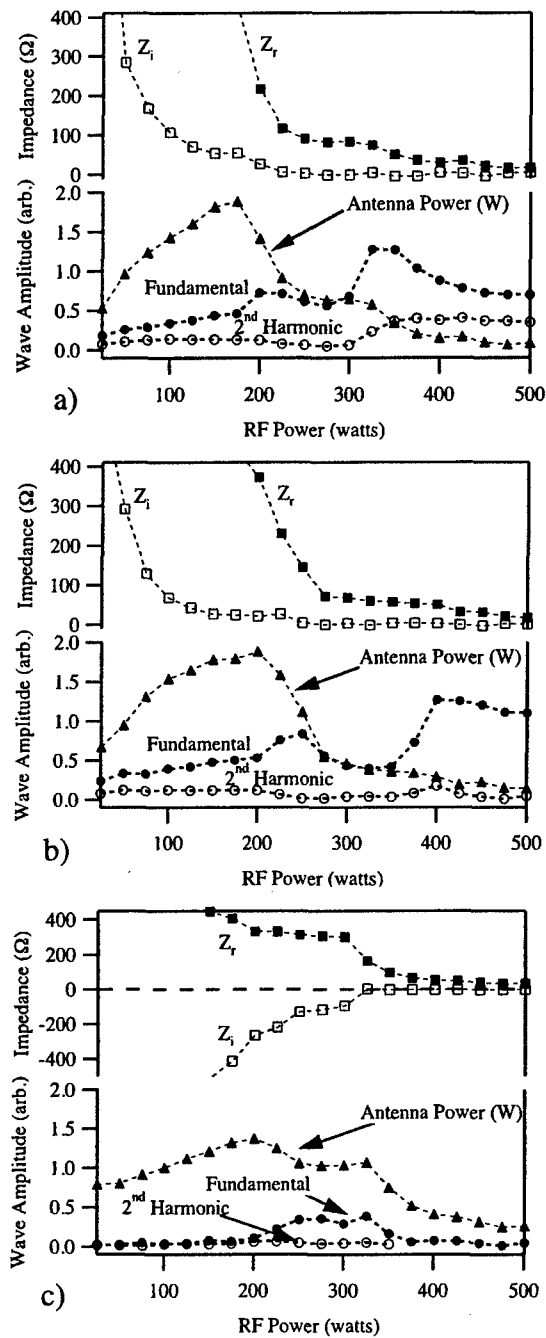


Figure 3.9: The amplitude of the launched wave as well as the impedance and the power delivered to the antenna plates are shown as functions of the rf power to the helicon antenna. The real and imaginary components of the antenna impedance are designated by  $Z_r$  and  $Z_i$  respectively. The fundamental as well as the second harmonic of the launched waves are measured with a Langmuir probe. a) Both plates are driven in phase (without the coupling capacitor). b) Both plates are driven in phase (with a coupling capacitor connected in series with the antenna, Fig. 3.7). c) The plates are driven out of phase.

power, and it does not seem to track the power delivered to the antenna plates. There are two maxima for the detected wave amplitude. One occurs at 200 – 250 W of rf power, when the real component of the measured impedance ( $Z_r$ ) approaches 150  $\Omega$ , the output impedance of the op-amp, and the imaginary part ( $Z_i$ ) is small. At that condition the entire circuit is matched. The second, and higher maximum occurs at 350–400 W of rf power, and probably corresponds to the increase in plasma density due to the transition from the inductive discharge mode to the helicon mode. The real part of the measured impedance at that point is 50  $\Omega$ . A more efficient wave launching can thus be achieved by choosing an amplifier with an impedance close to that value.

It is interesting to note that the Langmuir probe detected a plasma wave at the second harmonic aside the fundamental frequency driven by the circuit. As shown in Fig. 3.9 the second harmonic can be a significant fraction of the fundamental.

A similar experiment was repeated with the antenna plates driven out of phase. The results are shown in Fig. 3.9c. The maximum power delivered to the antenna in this case is about 75% of the power in the case described above. Also, the wave amplitude detected by the Langmuir probe is significantly lower than the amplitude of the wave launched by the plates driven in phase. Possible reasons as to why the out-of-phase configuration does not couple well into the plasma will be given in the next section. However as in the previous case, the maximum in the wave amplitude corresponds to the matched circuit condition,  $Z_i \ll Z_r \sim 150 \Omega$ , and not to the maximum power delivered to the antenna plates. The imaginary component of the impedance for the out-of-phase configuration is negative, indicating capacitive coupling between the plates. In the in-phase configuration the imaginary component is positive, indicating inductive coupling.

The in-phase driven antenna couples better to the plasma thus resulting in a wave with a higher amplitude than the out-of-phase driven antenna. We therefore undertook further study of the in-phase configuration. The goal of the study was to determine whether the launched wave is electrostatic in nature and whether it propagates transversely to the magnetic field.

### 3.6 Dispersion relation measurement

The electrostatic dispersion relation derived from the kinetic theory for an infinite slab of collisionless, homogeneous, isotropic, and non-drifting plasma can be written as [50, 30],

$$D = k_{\perp}^2 K_{xx} + k_{\parallel}^2 K_{zz} = 0, \quad (\text{A-1})$$

where  $k_{\perp}$  and  $k_{\parallel}$  are the perpendicular and the parallel components of the wavenumber, and  $K_{xx}$  and  $K_{zz}$  are two components of the dielectric tensor. For a single ion species plasma these components can be expressed as,

$$K_{xx} = 1 + \frac{\omega_{pe}^2}{\omega_{ce}^2} + \frac{\omega_{pi}^2 e^{-\lambda_i}}{k_{\parallel} \omega \lambda_i} \left( \frac{m_i}{2T_i} \right)^{1/2}$$

$$\times \sum_{n=-\infty}^{+\infty} n^2 I_n(\lambda_i) Z(\zeta_n^i), \quad (\text{A-2})$$

$$K_{zz} = 1 + \frac{2\omega_{pe}^2 m_e}{k_{\parallel}^2 2T_e} \times \left[ 1 + \frac{\omega}{k_{\parallel}} \left( \frac{m_e}{2T_e} \right)^{1/2} Z(\zeta_0^e) \right], \quad (\text{A-3})$$

where  $I_n$  is the modified Bessel function,  $\lambda_j = k_{\perp}^2 T_j / m_j \omega_{cj}^2$ ,  $Z(\zeta_n^j)$  is the plasma dispersion function [57], and  $\zeta_n^j = (\omega - n\omega_j)(m_j/2T_j)^{1/2}/k_{\parallel}$ , with  $j = e, i$ . In Eqs. (A-2)Eq:Kzz we assumed that  $\omega \ll \Omega_e$  and  $\lambda_e \ll 1$ .

To launch an electrostatic ion cyclotron (EIC) wave above the ion cyclotron frequency the following conditions must also be satisfied [50],

$$\begin{aligned} \omega_{pi} &> \omega_{ci}, \quad T_i \leq T_e, \\ (2T_i/m_i)^{1/2} &\ll \omega/k_{\parallel} \ll (2T_e/m_e)^{1/2}. \end{aligned}$$

In our experiment we have  $T_e = 3$  eV,  $T_i = 0.1$  eV,  $B = 261$  Gauss,  $\omega = 30 - 180$  kHz, and  $\lambda_{\parallel} \approx 46$  cm, therefore the above inequalities are satisfied. Here we assumed that the parallel wavelength is determined by the extent of the large glass cylinder where the waves are launched. By measuring the parallel component of the wavenumber with two axially separated Langmuir probes we have confirmed that the parallel wavenumber is  $\sim 46$  cm. The numerical solution of Eq. (A-1) for the plasma parameters in our experiment is represented in Fig. 3.10.

Theoretical curves can be subdivided into two types according to their slopes. One curve extending from  $k_{\perp} = 0$  to  $2 \text{ cm}^{-1}$  has a positive slope. This curve represents the forward branch of the EIC dispersion relation since its group velocity ( $\partial\omega/\partial k$ ) is in the same direction as its phase velocity ( $\omega/k$ ). On the other hand, curves extending from  $k_{\perp} = 1$  to  $6 \text{ cm}^{-1}$  have negative slopes. The curves correspond to cyclotron harmonics of the backward branch of the EIC dispersion relation, since their group velocity has the opposite sign of the phase velocity. The pass-band of each of these backward branches is narrow, and therefore we do not expect to see any of the backward mode waves propagating in our experiment.

The slope of the forward branch of the EIC dispersion is sensitive to the electron temperature, while the backward branch is sensitive to the ion temperature. Thus comparing the experimentally obtained dispersion relation to the theoretical expression provides a good check of the species temperatures. While the ion temperature was not measured, the electron temperature inferred by the slope of the experimental dispersion relation,  $T_e = 2.75$  eV, is in good agreement with the values measured independently with the rf-compensated Langmuir probe, shown in Fig. 3.5.

As was mentioned above, the theoretical dispersion relation given by Eq. (A-1) was derived for an idealized plasma. Some plasma parameters of our

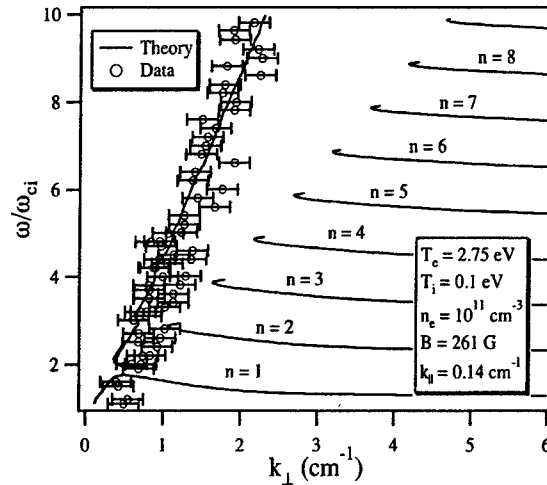


Figure 3.10: The measured dispersion relation at  $f_{ci}=10$  kHz agrees well with the theoretical dispersion for the forward branch of the Electrostatic Ion Cyclotron wave (EIC). Curves extending to large values of  $k_{\perp}$  represent the cyclotron harmonics of the EIC backward branch.

experiment are given by Fig. 3.6. It can be seen that the plasma is collisional ( $\nu_{ei}, \nu_{ii} > f_{ci}$ ). Also, the density profiles shown in Fig. 3.5 indicate that the plasma is not homogeneous,  $(a/n)\partial n/\partial x \geq 1$ , specifically at high rf power. Another point of concern is the effect of the plasma boundaries. At low values of  $k_{\perp}$  (long wavelength) the effect of the boundaries should be significant and the experimental data might diverge from the theoretical expression. With these considerations in mind, Fig. 3.10 shows a surprisingly good agreement between the experiments and the theory for a wide range of frequencies. The experimental data were obtained in the following manner.

A single wave was launched by the antenna plates inserted at the edge of the plasma column and driven in the in-phase configuration. We measured the wave dispersion by a system of three uncompensated Langmuir probes. The probes were placed orthogonally to each other so that simultaneous measurements of  $k_{\perp}$  and  $k_{\parallel}$  could be performed by measuring the signal delay between any two probes [58]. Measuring the probe signal with the plasma discharge off we determined that the ac-coupling signal was two orders of magnitude below the wave signal with the plasma turned on.

The parallel component of the wavenumber measured by the two probes placed along the magnetic field indicated that the parallel wavelength of the wave is 46 cm - the length of the large glass cylinder. This measurement was confirmed by the wave observations at various axial positions along the chamber. The perpendicular wavenumber, shown in Fig. 3.10, varies in accordance with the EIC dispersion. The dispersion measurements indicate that the wave is

propagating at the angle of  $82^\circ$  to  $86^\circ$  with respect to the magnetic field. Both the fundamental and the second harmonic components of the signal were used to construct the experimental dispersion relation shown in Fig. 3.10.

Driving the plates of the antenna out of phase, we expected the parallel wavelength to be 6.28 cm – twice the spacing between the plates. This however was not the case. The measured parallel wavelength was on the order of the chamber length. The measurements of the perpendicular wavelength were not consistent with the EIC dispersion relation. It is likely that the wave was affected by the ion Landau damping since  $w/k_{\parallel} \sim v_{thi}$ .

### 3.7 Conclusions regarding ES Wave Excitation

We reported on the excitation and propagation of an Electrostatic Ion Cyclotron (EIC) wave launched by a two-plate antenna into a magnetized argon plasma. We described in detail the circuitry necessary to drive the antenna in the in- and out-of-phase configuration.

We found that the antenna driven in phase couples better to the plasma and excites higher amplitude waves than the plates driven out of phase.

In addition, we determined that the wave amplitude can be optimized by carefully choosing the right plasma parameters and building a matched driving circuit.

The antenna driven in phase excites a wave with  $\lambda_{\parallel} = 46$  cm - the length of the portion of the vacuum chamber where the waves are launched. The perpendicular component of the wavenumber varies according to the EIC dispersion relation and is in good agreement with the forward branch of the theoretical dispersion relation despite the simplifying assumption of a collisionless, magnetized, homogeneous, isotropic, and infinite plasma slab. We found that EIC waves launched at frequencies between  $\omega_{ci}$  and  $10\omega_{ci}$  propagate with little damping at an angle between  $82^\circ$  and  $86^\circ$  with respect to the magnetic field.

Multiple EIC waves required for our ongoing beating waves studies [10, 25, 26, 21, 42] can also be easily launched by the plates antenna with two or more signal generators by means of a power combiner.

### 3.8 Demonstration of Ion Acceleration

After the success in launching the waves, we proceeded to measure the effects of the beating waves on ion acceleration to provide the first test for the existence of the new ion acceleration mechanism. The goal was to measure the ion's perpendicular energy (equivalently velocity or temperature) and observe if ion acceleration (or equivalently heating) occurs when a pair of beating ion cyclotron waves are launched. In order to do this measurement we developed, using funds from a recent DURIP grant, a dedicated state-of-the-art Laser Induced Fluorescence (LIF) diagnostic system (shown in Fig. (3.11)) that allows

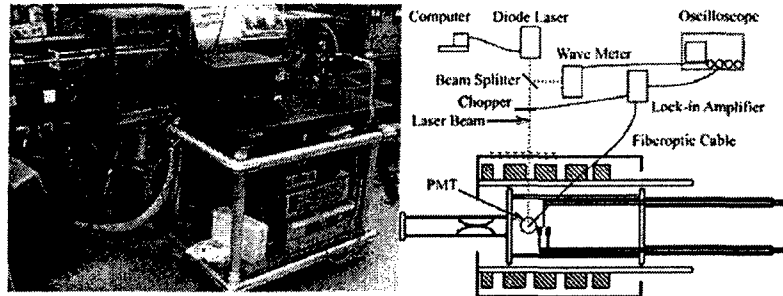


Figure 3.11: Photograph and schematic of the new state-of-the-art LIF system, recently developed under DURIP funding and used for our AFOSR-funded beating wave study.

accurate measurement of the ions' energy distribution function. Our LIF system is described in a recent publication ??.

The measurements led to the recently obtained results plotted in Fig. (3.12) which shows as much as 40% enhancement to the ion energy due to beating wave acceleration. **This represents the first experimental evidence ever of this new acceleration mechanism.**

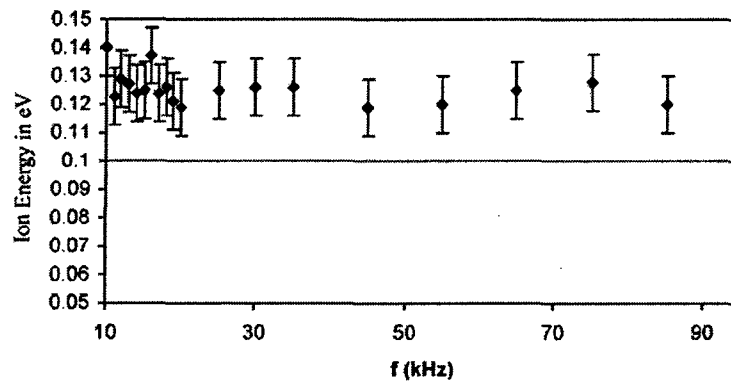


Figure 3.12: Measured ion energies (blue data points) under the effect of a pair of beating ion cyclotron waves compared to the benchmark case with no waves (red horizontal line at .1 eV) showing that the ions were accelerated by as much as 40%. (RF Power in helicon source = 250 W, Wave Antenna voltage = 60 V, ion cyclotron frequency = 10 kHz, wave frequency = 10-100 kHz.)

# Bibliography

- [1] A. Fukuyama, H. Mometa, R. Itatani, and T. Takizuka. Stochastic acceleration by an electrostatic wave near ion cyclotron harmonics. *Physical Review Letters*, 38:701, 1977.
- [2] G.R. Smith and A.N. Kaufman. Stochastic acceleration by a single wave in a magnetic field. *Phys. Rev. Lett.*, 34(26):1613, 1975.
- [3] C.F.F. Karney and A. Bers. Stochastic ion heating by a perpendicularly propagating electrostatic wave. *Physical Review Letters*, 39:550, 1977.
- [4] G.M. Zaslavsky, R.Z. Sagdeev, D.A. Usikov, and A.A. Chernikov. *Weak Chaos and Quasi-Regular Patterns*. Cambridge University Press, Cambridge, 1991.
- [5] C.F.F. Karney. Stochastic ion heating by a lower hybrid wave. *Physics of Fluids*, 21(9):1584-1599, 1978.
- [6] F. Skiff, F. Anderegg, and M.Q. Tran. Stochastic particle acceleration in an electrostatic wave. *Phys. Rev. Lett.*, 58(14):1430, April 1987.
- [7] D. Benisti, A.K. Ram, and A. Bers. Ion dynamics in multiple electrostatic waves in a magnetized plasma. I. Coherent acceleration. *Phys. Plasma*, 5(9):3224, September 1998.
- [8] D. Benisti, A.K. Ram, and A. Bers. Ion dynamics in multiple electrostatic waves in a magnetized plasma. II. Enhancement of the acceleration. *Phys. Plasma*, 5(9):3233, September 1998.
- [9] A.K. Ram, A. Bers, and D. Benisti. Ionospheric ion acceleration by multiple electrostatic waves. *J. Geophys. Res.*, 103:9431, 1998.
- [10] E.Y. Choueiri and R. Spektor. Coherent ion acceleration using two electrostatic waves. Presented at the 36<sup>th</sup> AIAA Joint Propulsion Conference, Huntsville, AL, July 16-20, 2000. AIAA-2000-3759.
- [11] R. Grimshaw. *Nonlinear Ordinary Differential Equations*. Blackwell Scientific Publications, Oxford, 1990.

- [12] A.J. Lichtenberg and M.A. Lieberman. *Regular and Chaotic Motion*. Addison-Wesley, Cambridge, MA, 1983.
- [13] Ping-Kun Chia, L. Schmitz, and R.W. Conn. Stochastic ion behavior in subharmonic and superharmonic electrostatic waves. *Phys. Plasmas*, 3(5):1545, May 1996.
- [14] H. Goldstein. *Classical Mechanics*. Addison-Wesley, Cambridge, MA, 1951.
- [15] A. Deprit. *Celest. Mech.*, 1:12, 1969.
- [16] J.R. Cary. *Phys. Rep.*, 79:129, 1981.
- [17] R. Candy and W. Rozmus. A symplectic integration algorithm for separable hamiltonian functions. *J. Comp. Phys.*, 92:230, 1991.
- [18] R. Candy and W. Rozmus. Rational resonances in a wave driven linear oscillator. *Physica D*, 52:267, 1991.
- [19] D. Benisti, A.K. Ram, and A. Bers. Lower bound in energy for chaotic dynamics of ions. *Phys. Lett. A*, 233:209, August 1997.
- [20] Ping-Kun Chia, L. Schmitz, and R.W. Conn. Effect of elastic scattering on stochastic ion heating by electrostatic waves. *Phys. Plasmas*, 3(5):1569, May 1996.
- [21] R. Spektor and E.Y. Choueiri. Effects of ion collisions on ion acceleration by beating electrostatic waves. Presented at the 28<sup>th</sup> International Electric Propulsion Conference (IEPC), Toulouse, France March 17-21, 2003. IEPC-03-65.
- [22] G.N. Watson. *A Treatise on the Theory of Bessel Functions*. Cambridge University Press, Cambridge, 2 edition, 1962.
- [23] D.J. Strozzi, A.K. Ram, and A. Bers. Coherent acceleration of magnetized ions by electrostatic waves with arbitrary wavenumbers. *Phys. Plasmas*, 10(7):2722-2731, March 2003.
- [24] G.M. Zaslavsky, R.Z. Sagdeev, D.A. Usikov, and A. A. Chernikov. Minimal chaos, stochastic webs, and structures of quasicrystal symmetry. *Usp. Fiz. Nauk*, 156(193-251):887, October 1988.
- [25] R. Spektor and E.Y. Choueiri. Ion acceleration by beating electrostatic waves: Criteria for regular and stochastic acceleration. Presented at the 27<sup>th</sup> International Electric Propulsion Conference (IEPC), Pasadena, California October 14-19, 2001. IEPC-01-209.
- [26] R. Spektor and E.Y. Choueiri. Design of an experiment for studying ion acceleration by beating waves. Presented at the 38<sup>th</sup> AIAA/ASME/SAE/ASEE Joint Propulsion Conference (JPC), Indianapolis, Indiana, July 7-10, 2002.

- [27] T. Takizuka and H. Abe. A binary collision model for plasma simulation with a particle code. *J. Comp. Phys.*, 25:205-219, 1977.
- [28] R. Boswell and F.F. Chen. Helicons - the past decade. *IEEE Trans. Plasma Sci.*, 25(6):1245, December 1997.
- [29] R. Boswell and F.F. Chen. Helicons - the early years. *IEEE Trans. Plasma Sci.*, 25(6):1229, December 1997.
- [30] T.H. Stix. *Waves in Plasmas*. Springer-Verlag, New York, 1992.
- [31] D.G. Swanson. *Plasma Waves*. Academic Press, Boston, 1989.
- [32] N. J. Fisch. Confining a tokamak plasma with rf-driven currents. *Phys. Rev. Lett.*, 41(13):873, September 1978.
- [33] E.A. Bering III, M. Brukhardt, F.R. Chang-Diaz, V. Jacobson J.P. Squire, R.D. Bengtson, J.N. Gibson, and T. Glover. Experimental studies of the exhaust plasma of the vasimr engine. Presented at the 40<sup>th</sup> Aerospace Sciences Meeting, Reno, Nevada January ,14-17 2002, AIAA 2002-0345.
- [34] D.G. Chavers and F.R. Chang-Diaz. Momentum flux measuring instrument for neutral and charged particle flows. *Rev. Sci. Instrum.*, 73(10):3500, October 2002.
- [35] F.R. Chang-Diaz, J.P. Squire, T. Glover, A.J. Petro, E.A. Bering III, F.W. Baity, R.H. Goulding, M.D. Carter, R.D. Bengtson, and B.N. Breizman. The vasimr engine: Project status and recent accomplishments. Presented at the 42<sup>nd</sup> Aerospace Sciences Meeting, Reno, Nevada January ,5-8 2004, AIAA 2004-0149.
- [36] E.G. Shelley, R.D. Sharp, and R.G. Johnson. Satellite observations of an ionospheric acceleration mechanism. *J. Geophys. Res.*, 3(11):654, 1976.
- [37] Mozer F.S., C.W. Carlson, M.K. Hudson, R.B. Torbert, B. Parady, and J. Yatteau. Observations of paired electrostatic shocks in the polar magnetosphere. *Phys. Rev. Lett.*, 38(6):292, 1977.
- [38] A.G. Ghielmetti, R.G. Johnson, R.D. Sharp, and E.G. Shelley. The latitudinal, diurnal, and altitudinal distributions of upward flowing energetic ions of ionospheric origin. *Geophys. Res. Lett.*, 5(1):59, 1978.
- [39] P.M. Kintner, M.C. Kelley, R.D. Sharp, A.G. Ghielmetti, M. Temerin, C. Cattell, P.F. Mizera, and J.F. Fennell. Simultaneous observations of energetic (keV) upstreaming and electrostatic hydrogen cyclotron waves. *J. Geophys. Res.*, 84(A12):7201, 1979.
- [40] P. Satyanarayana, P.K. Chaturvedi, M.J. Keskinen, J.D. Huba, and S.L. Ossakow. Theory of the current-driven ion cyclotron instability in the bottomside ionosphere. *J. Geophys. Res.*, 90(A12):12,209, 1985.

- [41] R. Spektor and E. Y. Choueiri. Ion acceleration by beating electrostatic waves: Domain of allowed acceleration. *Physical Review, E*, 69(4):Article No. 046402, 2004.
- [42] R. Spektor and E.Y. Choueiri. Ion acceleration by beating electrostatic waves: Domain of allowed acceleration. *Phys.Rev.E*, 69(4):046402, April 2004.
- [43] R.W. Motley and N. D'Angelo. Excitation of electrostatic plasma oscillations near ion cyclotron frequency. *Phys. Fluids.*, 6(2):296, February 1963.
- [44] D.M. Suszcynsky, S.L. Cartier, R.L. Merline, and N. D'Angelo. A laboratory study of collisional electrostatic ion cyclotron waves. *J. Geophys. Res.*, 91(A12):13,729, December 1986.
- [45] D.N. Walker, , W.E. Amatucci, G. Ganguli, J.A. Antoniadis, J.H. Bowles, D. Duncan, V. Gavrishchaka, and M.E. Koepke. Perpendicular ion heating by velocity-shear-driven waves. *Geoph.Res. Lett.*, 24(10):1187, May 1997.
- [46] W.M.Hooke and S.Bernabei. Direct observation of waves propagating near the lower-hybrid-resonance frequency. *Phys.Rev.Lett.*, 28(7):407, February 1972.
- [47] R.L.Stenzel and W.Gekelman. Electrostatic waves near the lower hybrid frequency. *Phys.Rev. A*, 11(6):2057, June 1975.
- [48] J.P.M. Schmitt. Dispersion and cyclotron damping of pure ion Bernstein waves. *Phys.Rev.Lett.*, 31(16):982, October 1973.
- [49] J.P.M. Schmitt and P. Krumm. Mode conversion and plasma column resonances in the ion-cyclotron harmonic range. *Phys.Rev.Lett.*, 37(12):753, September 1976.
- [50] J. Goree, M. Ono, and L. K. Wong. Observation of the backward electrostatic ion-cyclotron wave. *Phys. Fluids*, 28(9):2845, September 1985.
- [51] J.L. Kline. Resonant ion heating in a helicon plasma. Ms, West Virginia University, 1998.
- [52] J. Kline, E. Scime, P.A. Keiter, M.M. Balkey, and R.F. Boivin. Ion heating in the helix helicon plasma source. *Phys.Plasmas*, 6(12):4767-4772, December 1999.
- [53] G.A. Goree. *The backward electrostatic ion-cyclotron wave, fast wave current drive, and fir laser scattering*. Ph.d, Princeton University, 1985.
- [54] R. Sudit and F. F. Chen. Rf compensated probes for high-density discharges. *Plasma Sources Sci. Technol*, 3:162-168, 1994.
- [55] J.G.Laframboise. Technical Report 100, University of Toronto, Institute for Aerospace Studies, 1966. Document No. AD634596.

- [56] F.F.Chen and J.D. Evans and D.Arnush. A floating potential method for measuring ion density. *Phys.Plasas*, 9(4):1449, April 2002.
- [57] B.D. Fried and S.D. Conte. *The plasma dispersion function ; the Hilbert transform of the Gaussian*. Academic Press, New York, 1961.
- [58] D.E. Smith, E.J. Powers, and G.S. Cladwell. Fast-fourier-transform spectral-analysis techniques as a plasma fluctuation diagnostic tool. *IEEE Trans. Plasma Sci.*, PS-1:261, December 1974.

## Impact Statement

The revised budget represents about two-thirds the original budget. Therefore, the scope of the work will be adjusted as follows.

The original plan was to explore the use of three different layered materials: bismuth telluride, bismuth selenide, and molybdenum diselenide. However, in view of the reduced budget, we will concentrate on the first and last as the first two are quite similar. I do not think this will seriously affect the scientific understanding of nanocomposites we expect from this study.